Geochimica et Cosmochimica Acta 337 (2022) 140–154

Contents lists available at ScienceDirect

Geochimica et Cosmochimica Acta

journal homepage: www.elsevier.com/locate/gca

Reconstructing the lithium isotopic composition (δ^7Li) of seawater from shallow marine carbonate sediments

Jack G. Murphy [a,*], Anne-Sofie C. Ahm [a,b], Peter K. Swart [c], John A. Higgins [a]

[a] Department of Geosciences, Princeton University, United States
[b] School of Earth and Ocean Science, University of Victoria, BC, Canada
[c] Rosentiel School of Marine and Atmospheric Science, University of Miami, United States

ARTICLE INFO

Article history:
Received 12 February 2022
Accepted 16 September 2022
Available online 23 September 2022
Associate editor: Alexandra V. Turchyn

Keywords:
Carbonate geochemistry
Carbonate diagenesis
Lithium isotopes
Seawater chemistry
Dolomitization

ABSTRACT

Records of the lithium isotopic composition of seawater (δ^7Li_{sw}), preserved in the lithium isotopic composition of shallow-marine carbonate sediments (δ^7Li_{carb}), provide information about the links between silicate weathering and clay formation, the global carbon cycle, and Earth's climate on geologic timescales. However, the record of δ^7Li_{sw} values in shallow marine carbonates is complicated by the effects of mineralogy (e.g., calcite vs aragonite) and diagenesis. Here we present measurements of bulk carbonate δ^7Li values paired with a suite of stable isotope systems ($\delta^{44/40}$Ca, δ^{26}Mg) and element abundance ratios (Li/(Ca + Mg), Sr/(Ca + Mg), Mg/(Ca + Mg)) in Neogene shallow-marine carbonates from sites in the Bahamas and southwest Australia. The studied sites span a range of depositional and diagenetic settings and exhibit large stratigraphic trends in δ^7Li values that correlate with mineralogy, $\delta^{44/40}$Ca values, and/or element abundances. These trends differ from coeval planktonic foraminifera records of δ^7Li_{sw} and instead predominantly reflect local processes. We show, using a suite of geochemical analyses and a numerical model of early marine diagenesis, that the observed variability in bulk sediment δ^7Li values can be quantitatively explained by the effects of mineralogy and diagenetic alteration under both fluid-buffered and sediment-buffered conditions. Using this framework, we show that it is possible to produce robust and accurate 'snapshots' of the δ^7Li value of seawater in the geologic past from shallow-water marine carbonate sediments.

1. Introduction

Establishing records of the geochemical fluxes that control Earth's carbon cycle on million-year time scales is essential to understanding the underlying causes of climate variability over Earth History. Central to the global carbon cycle is the breakdown and formation of silicate minerals. Weathering of continental silicate rocks, high temperature hydrothermal activity at oceanic spreading centers, low-temperature off-axis seafloor alteration, and clay authigenesis in oceanic sediment are all linked to Earth's surface temperature and pCO_2. As lithium is predominantly hosted in silicate minerals and the fractionation of lithium isotopes (^{7}Li/^{6}Li ratio or δ^7Li values) is controlled principally by the formation of secondary silicate minerals (e.g., clays), the δ^7Li value of seawater (δ^7Li_{SW}) has emerged as a promising tracer for reconstructing the cycling of silicate minerals at Earth's surface over geologic history (Hathorne and James, 2006; Misra and Froelich, 2012; Pogge von Strandmann et al., 2013; Pogge von Strandmann et al., 2020; Washington et al., 2020; Kalderon-Asael et al., 2021). Reconstructions from planktonic foraminifera (Hathorne and James 2006; Misra and Froelich, 2012) and brachiopods (Washington et al., 2020) indicate a significant rise (~9‰) in δ^7Li_{sw} values over the last 60 Myrs, coincident with changes in Earth's surface temperature, seawater chemistry, and pCO_2. However, such fossil archives are limited in their potential to extend the record of δ^7Li_{SW} throughout Earth history as a result of changes in vital effects (Vigier et al., 2015; Roberts et al., 2018; Bastian et al., 2018) and the rarity (or total absence) of well-preserved fossils in Mesozoic and older sediments.

Shallow-marine carbonate rocks are one of the most widely used archives of the history of seawater chemistry as marine carbonate sediments are abundant, span 3 + billion years of Earth history, and have chemical and isotopic compositions interpreted to reflect the fluid from which they precipitated, e.g., ancient seawater (Morse and Mackenzie, 1990; Jacobsen and Kaufman, 1999; Veizer et al., 1999; Shields and Veizer, 2002). A number of studies have interpreted stratigraphic variability of δ^7Li values in shallow-water marine carbonates as recording secular change in

* Corresponding author.
E-mail address: jackmurphy@princeton.edu (J.G. Murphy).

https://doi.org/10.1016/j.gca.2022.09.019
0016-7037/

contemporaneous δ^7Li_{SW} values resulting from variation in the magnitude and/or isotopic composition of lithium fluxes to/from the ocean (Pogge von Strandmann et al., 2013; Lechler et al., 2015; Pogge von Strandmann et al., 2017, Sproson et al. 2022). However, studies of modern and recent shallow-water carbonate sediments have shown that mineralogy and early marine diagenesis play an important role in determining the chemical composition of shallow-water carbonate sediments and their stratigraphic expression in the geologic record (Bathurst, 1966, 1971; Morse and MacKenzie, 1990; Higgins et al., 2018, Fantle et al., 2020). This problem is particularly acute for Li isotopes in bulk shallow-water marine carbonates as there are large (~5 to 12 ‰) isotopic effects associated with both mineralogy (e.g., aragonite vs calcite; Marriott et al., 2004a,b; Hall et al., 2005; Hathorne and James 2006; Misra and Froelich, 2009; Rollion-Bard et al., 2009; Vigier et al., 2015; Dellinger et al., 2018; Pogge von Strandmann et al., 2019, Day et al., 2021) and diagenesis (marine and meteoric; Dellinger et al., 2020). These observations highlight the need for a robust method to disentangle geochemical signals associated with mineralogy and diagenesis from signals associated with secular changes in the δ^7Li value of seawater.

Here we present a large dataset of δ^7Li values of Neogene marine carbonates from a range of depositional settings (platform top, platform mid-slope, platform deep-slope, continental margin) paired with major-element isotope ratios ($\delta^{44/40}$Ca, δ^{26}Mg) and element ratios (Li/(Ca + Mg), Sr/(Ca + Mg), Mg/(Ca + Mg)). We place the lithium isotope data within an established framework and model of carbonate diagenesis (Ahm et al., 2018; Blättler et al., 2015; Crockford et al., 2021; Fantle and Higgins, 2014; Higgins et al., 2018; Murray et al., 2021) that uses covariations of $\delta^{44/40}$Ca, δ^{26}Mg, δ^{13}C, δ^{18}O, and element ratios to fingerprint primary mineralogy (aragonite, calcite), diagenetic setting (meteoric, marine), extent and style of early diagenesis (fluid-buffered vs sediment-buffered), and diagenetic fluid composition. This framework has been successfully applied to both modern and ancient carbonates and provides a template for establishing precise 'snapshots' of seawater δ^7Li values over Earth History.

2. Site description

The eleven sites studied (Figs. 1 and 2) represent a range of dominant carbonate mineralogy (aragonite, high-Mg calcite (HMC), low-Mg calcite (LMC), dolomite) and depositional setting (platform bank-top, margin, slope). Our sample suite includes surface sediment and eight core sites from carbonate platform and slope environments in the Bahamas collected during various drilling campaigns. In chronological order these included a core from San Salvador (Supko, 1977; Dawans and Swart, 1988), cores drilled on the Little Bahama Bank (LBB) (Vahrenkamp et al., 1991), cores (Clino and Unda) drilled on the western margin of Great Bahama Bank (GBB) (Ginsburg, 2001), and finally-two sites (Site 1003 and Site 1007) drilled during the Leg 166 of the Ocean Drilling Program (ODP) (Eberli et al., 1996). We also analyzed samples of surface sediment from Triple Goose Creek on north-west Andros Island and Joulter Cays, Bahamas. A ninth core is from ODP Site 1131 on the uppermost slope of the Eucla Shelf in the Great Australian Bight (Feary et al., 2000). Finally, we analyzed 32 seawater samples from the Great Bahamas Bank (Geyman and Maloof, 2019) and transects of the North Atlantic and South Pacific at depths ranging from surface to 4000 mbsl (Marconi et al., 2019).

2.1. The Bahamas

Shallow water sediments in the Bahamas are composed primarily of non-skeletal aragonite (ooids and peloids) with minor amounts of bioclastic LMC and HMC (Swart et al., 2009). The diagenetic history of the Bahamas consists of periods of both marine and meteoric alteration. Throughout the Neogene the platforms were subject to the influence of variable sea level associated with glacial cycles (Eberli and Ginsburg, 1987; Eberli et al., 1997; Kievman 1998; Ginsburg, 2001). Pleistocene sea-level reached a minimum of ~130 m below modern sea-level (Lisiecki and Raymo, 2005) allowing meteoric fluids to penetrate to a depth of at least 200 m at Clino and 108 m at Unda (Swart and Oehlert, 2018). Samples from below these depths are the focus of this study where sediments have been subjected to marine diagenesis including dolomitization (Higgins et al., 2018).

2.1.1. Surface Sediment

Carbonate surface samples were collected from two locations: Joulter Cays, an ooid sand shoal located on the margin of the Great Bahama Bank north of Andros Island, and from Triple Goose Creek, a carbonate tidal flat located on north-west Andros Island. We also compiled previously published element ratio and isotope (δ^7Li, $\delta^{44/40}$Ca, δ^{26}Mg, δ^{13}C, δ^{18}O) data from Triple Goose Creek (Higgins et al., 2018), sites near the Exuma Cays on the eastern margin of the Great Bahama Bank (Zhang et al., 2017; Pogge von Strandmann et al., 2019), and a grid across the Great Bahama Bank (Swart et al., 2009) to estimate a representative geochemistry of modern Bahamas surface sediment.

2.1.2. GBB (Bahamas Drilling Projects Sites Unda, Clino, and ODP Site 1003)

Samples from GBB come from three sites drilled into the current platform top (Unda), margin (Clino), and slope (ODP Site 1003) (Eberli and Ginsburg, 1987; Eberli et al., 1997). A brief review of sedimentology and stratigraphy of each site is presented here while more detailed descriptions can be found in previous publications (e.g., Eberli, 2000; Ginsburg, 2001; Kenter et al., 2001; McNeill et al., 2001; Melim et al., 2004; Murray et al., 2021; Murray and Swart, 2017; Swart and Melim, 2000; Eberli et al., 1997).

Core Unda consists of shallow-water platform and reefal deposits that alternate with deeper marginal deposits (Kenter et al., 2001). Sediments at Unda have seen a wide range of diagenetic conditions. Above 108 m, sediment shows evidence of meteoric diagenesis including erosional surfaces, low δ^{13}C and δ^{18}O values, and LMC dominated mineralogy (Melim et al., 2001). Below this depth marine hard grounds represent hiatuses in sedimentation and prolonged exposure of sediments to diagenesis by marine fluids. Dolomite abundance increases with depth to a fully dolomitized interval between 270 and 345 mbsf. Strontium isotopes ($^{87}Sr/^{86}Sr$) suggest dolomitization driven by reaction with seawater was either contemporaneous or within a few million years of deposition (Swart et al., 2001).

Core Clino contains three major lithological units representing distinct depositional setting. The upper 200 m of the core contains sediment deposited on the shallow-water platform top and reefs, which was subaerially exposed and altered by meteoric fluids during the glacially-induced sea-level low stands of the Pleistocene. The middle interval (200–370 mbsf) represents upper slope deposits, while the deeper interval (370–700 mbsf) contains lower slope deposits. A major erosional boundary at 367 mbsf and a hardground at 537 mbsf represent multi-million year depositional hiatuses (Kenter et al., 2001). The carbonate mineralogy of Clino varies significantly with depth. Between 34 and 150 mbsf, sediment is composed predominantly of LMC. In the underlying interval (150–364 mbsf), aragonite sediment is abundant, composing up to 65 wt% of the bulk sediment. Below 367 mbsf, dolomite becomes a significant component, with the highest proportions occurring directly below the erosional boundary at 367 mbsf and hardground

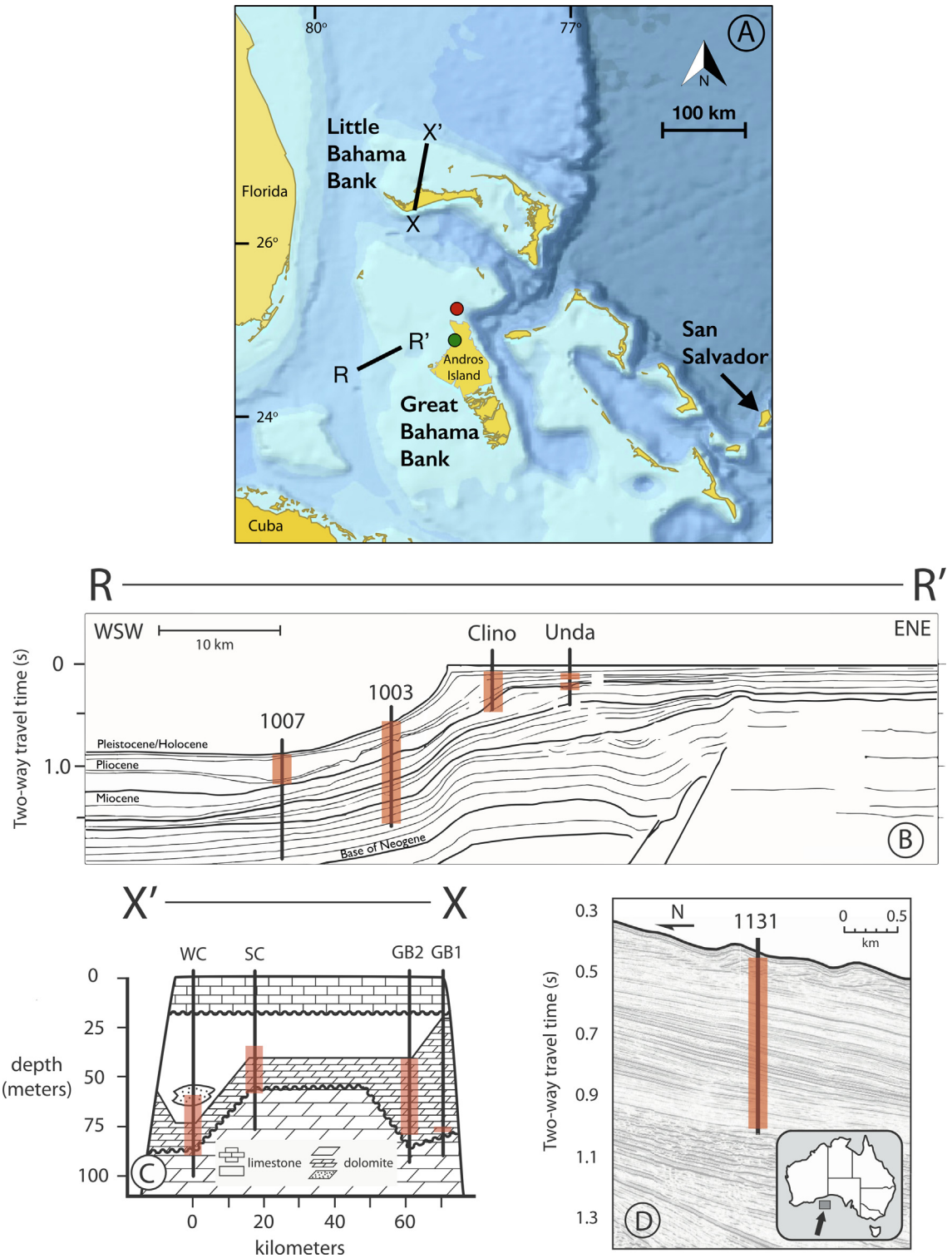

Fig. 1. Maps of sites used in this study. (A) Transects and study sites from the Bahamas. Lines R-R' and X-X' denote transects; circles denote surface sediment sample sites Triple Goose Creek (green) and Joulter Cays (red). (B) Transect along the western flank of the Great Bahama Bank. Shaded intervals denote depths at which samples used in this study were taken. (C) Transect from the Little Bahama Bank. Shaded intervals denote depths at which samples used in this study were taken. Lithologies of predominantly limestone vs dolomite are indicated. (D) Site 1131 from the Eucla shelf in southwest Australia. Shaded interval denotes depths at which samples used in this study were taken. (For interpretation of the references to colour in this figure legend, the reader is referred to the web version of this article.)

at 536 mbsf. Petrographic evidence (Swart and Melim, 2000) and strontium isotopes ($^{87}Sr/^{86}Sr$) (Swart et al., 2001) suggest the timing of dolomitization is contemporaneous with or within 2 My of deposition.

Ocean Drilling Program Site 1003 was drilled into the middle slope (483 m below sea level) of the GBB. The cores record approximately 1300 m of carbonate sedimentation onto the mid-slope from the Early Miocene to the Pleistocene (Eberli et al., 1997). Carbonate sediment at the site is primarily sourced from the platform top (aragonite) with variable contribution from pelagic carbonate (LMC). Within the upper 100 m, carbonate mineralogy is aragonite with lesser amounts of HMC and dolomite and is

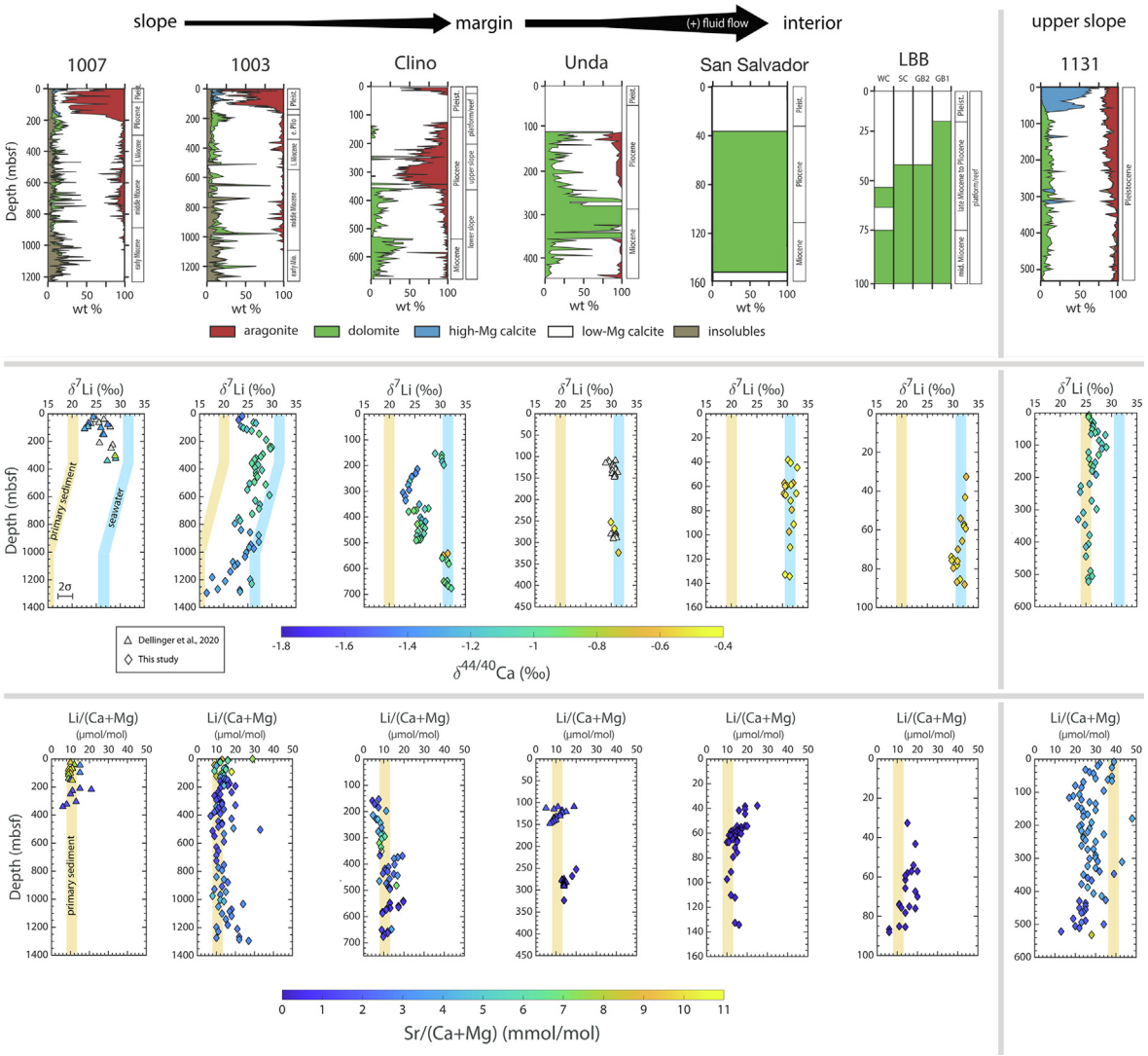

Fig. 2. Depth profiles of bulk sediment mineralogy (TOP), δ^7Li values (MIDDLE) and Li/(Ca + Mg) ratios (BOTTOM) for all studied core sites. TOP: Aragonite is abundant in the upper ~200 m at Sites 1007 and 1003 whereas peak aragonite abundance occurs at ~300 m at Clino. Aragonite is a minor component or absent from studied samples from Unda, San Salvador, and LBB, and is a minor component at Site 1131, where the dominant primary metastable carbonate is HMC. Dolomite abundance increases from slope to platform margin and interior, and near hardgrounds and erosional surfaces. MIDDLE: Measured δ^7Li values are colored by bulk sediment $\delta^{44/40}$Ca values. Triangle symbols at Sites 1007 and Unda are from Dellinger et al., 2020 and most have not been analyzed for Ca isotopes. All other samples were analyzed at Princeton University. Shaded regions indicate contemporaneous seawater (blue) and primary sediment (tan) δ^7Li values inferred from independent archives of seawater δ^7Li values (Hathorne and James, 2006; Misra and Froelich, 2012; Washington et al., 2020). Surface sediment is dominated by aragonite for all Bahamas sites and by HMC for Site 1131. BOTTOM: Measured Li/(Ca +Mg) ratios are colored by bulk sediment Sr/(Ca+Mg) ratios. Shaded regions indicate Li/(Ca+Mg) ratios for measured bank-top sediment (Bahamas) or core top sediment (1131). (For interpretation of the references to colour in this figure legend, the reader is referred to the web version of this article.)

mostly unlithified. Below this, the percentage of preserve aragonite decreases significantly and HMC disappears while sediment become partially to fully lithified. Dolomite becomes a more significant, though minor, component of the carbonate sediment for much of the core below 110 m and is commonly found at higher proportions below non-depositional surfaces.

2.1.3. Little Bahama Bank (WC1, SC1, GB2, and GB1)

The Little Bahama Bank (LBB) hosts a sequence of massive dolomite bodies at relatively shallow depths (20–100 mbsf) in outer-reef and inner-platform sediments of Neogene age. Here we study-four cores drilled along a N—S transect of the platform: Grand Bahamas Island (GB1 & GB2), Sales Cay (SC), and Walkers Cay (WC1) (Vahrenkamp et al., 1991). Strontium isotope measurements indicate three distinct phases of dolomitization by unaltered seawater in the Late Miocene, Late Pliocene, and Early Pleistocene (Vahrenkamp et al., 1988, 1991). In this paper we focus on samples dolomitized in the Late Pliocene.

2.1.4. San Salvador

A 169 m core was drilled into San Salvador island penetrating Pleistocene to Miocene aged carbonates including a massive dolomite body between 35 and 145 mbsf (Supko 1977; Swart et al., 1987; McNeill et al., 1988). Strontium isotopes and uranium disequilibrium series dating suggest LMC was dolomitized during at least two episodes. It appears that active dolomitization has continued within the Pliocene section of the core as recently as 150 ka, highlighting potential for dolomitization to continue several million years post deposition (Swart et al., 1987).

2.2. Australia

2.2.1. Eucla Shelf (Ocean Drilling Program Site 1131)

In contrast to the warm water environment of the Bahamas where surface sediment mineralogy is predominantly aragonite, the Eucla shelf is a cool water environment with large proportion of surface sediments composed of HMC. Ocean Drilling Program

Site 1131 is located adjacent to the Eucla shelf and drilled into the upper continental slope 332 m below sea level (Fig. 1D). The core captures late-Pliocene to Pleistocene aged sediment deposited rapidly (accumulation rates ~ 25 cm/ky). The upper 70 m of the core contains a significant fraction of HMC which declines downcore mirrored by a commensurate increase in LMC and the appearance of dolomite (20–30 %). Aragonite is also present throughout the core as a minor constituent (<10 %) (Feary et al., 2000).

3. Methods

3.1. Sample preparation

Approximately 20 mg bulk carbonate powders were drilled from carbonate samples avoiding obvious veins, fractures, bioclasts, or other impurities. Sample powders were leached in 15 ml of 0.25 M buffered acetic acid (pH ~ 5 using ammonium hydroxide buffer), ultrasonicated for 4 h, then centrifuged at 2500 rpm for 30 min. The supernatant was transferred to clean Teflon vials, evaporated to dryness at a temperature of 60–80 °C, and re-dissolved in 1 ml of 1 N HNO_3 for ion chromatography.

As silicate minerals contain high concentrations of Li relative to carbonate minerals (typically > 20 ppm vs < 5 ppm, respectfully) and substantially lower lithium isotopic composition (typically < 10 ‰ vs > 20 ‰, respectfully) (Chan et al., 2006; Tomascak et al., 2016; Penniston-Dorland et al., 2017), minor proportions of silicate minerals can influence the lithium isotopic composition of bulk sample leachates. We therefore employ a weak acetic acid digestion to minimize silicate contamination (Taylor et al., 2019; Lin et al., 2019). Further, we monitor sample leachates for elevated aluminum and lithium content associated with depressed δ^7Li values as indication of silicate-bound lithium contamination (Fig. S2). In cases where such a correlation is clearly defined, possible silicate contamination is discussed, however no samples are excluded on the basis of a threshold value.

3.2. Element ratio analysis

Aliquots of sample leachates were measured for elemental ratios on a ThermoScientific iCAP-Q ICP-MS at Princeton University. Samples were analyzed at a calcium concentration of 100 ppm and calibration curves of matrix-matched standards bracketed the concentrations of elements in the sample solutions (Rosenthal et al., 1999). The external reproducibility of Me/(Ca + Mg) ratios are determined from long-term replicate measurements of SRM88b, a dolomitic limestone, yielding an estimated precision of ±5–7 % (2σ).

3.3. Ion chromatography

Calcium was isolated from matrix elements using an automated Dionex ICS-5000 + ion chromatography (IC) system coupled with a Dionex AS-AP fraction collector following a previously published protocol (Blättler et al., 2015; Husson et al., 2015; Gothmann et al., 2016; Higgins et al., 2018).

Lithium was separated from the matrix elements by gravity driven ion-exchange chromatography. Savillex™ microcolumns (30 ml reservoir, 25 cm capillary length, 6.4 mm internal diameter) were loaded with 5.5 ml of Bio-Rad AG50W X-12 (100–200 mesh) resin. The resin was washed with 15 ml of 6 N HNO_3, rinsed with 10 ml MilliQ™ water, and conditioned with 10 ml 0.5 N HCl. Dissolved samples (in 1 ml 1 N HNO_3) were loaded onto the resin and eluted with 0.5 M HCl. The lithium fraction (14–43 ml) was collected then evaporated to dryness at 60-80℃. Remaining matrix elements were stripped from the resin by passing 15 ml 6 N HNO_3 followed by a 10 ml MilliQ water rinse. To ensure complete separation of Li and Na, the sample was passed through the entire procedure a second time.

Purified calcium and lithium samples were treated with concentrated (16 N) HNO_3, dried, and re-dissolved in 2 % HNO_3 for isotope analysis.

3.4. Isotope Ratio Mass spectrometry

Isotope ratio analyses were performed on a Neptune Plus MC-ICP-MS at Princeton University. All data are reported in delta notation relative to a known, internationally available, standard. Long-term external reproducibility for each isotope system is determined based on two known standards processed through the entire chemical procedure with every batch of 18 samples. All uncertainty is reported with 2σ standard deviation unless otherwise noted.

Calcium isotope ratios were measured using a previously published method (Blättler and Higgins, 2014; Fantle and Higgins, 2014; Blättler et al., 2015; Husson et al., 2015; Gothmann et al., 2016; Higgins et al., 2018). Measured $\delta^{44/42}$Ca values were converted to $\delta^{44/40}$Ca, assuming mass-dependent fractionation with slope 2.05 and no excess radiogenic ^{40}Ca (Fantle and Tipper, 2014), and reported relative to modern seawater ($\delta^{44/40}Ca_{seawater}$ = 0 ‰; $\delta^{44/40}Ca_{seawater}$=+1.92 ‰ on the SRM915a scale). Processed Ca standards included both SRM915b and seawater with a long term measured offset between the two of −1.18 ± 0.16 ‰ (2σ; N = 125). We therefore consider the external precision of our calcium isotope measurements to be ± 0.16 ‰ (2σ).

Lithium isotopes were measured using an ESI Apex-IR sample introduction and desolvation system with 100 μL/min PFA nebulizer, hot plasma (1200 W), at low resolution using X skimmer and Jet sampler cones. Sample were measured against an in-house isotope standard (HPS: δ^7Li_{HPS} = −12.13 ± 0.04 ‰ relative to LSVEC, 2SE, n = 143) using beam intensities ^{7}Li and ^{6}Li on cups H4 and L4, respectively. A typical ^{7}Li signal intensity was approximately 2–3 V for a 5 ppb Li solution. Lithium isotope ratios are reported relative to international lithium standard LSVEC (NIST SRM 8545) using $\Delta_{LSVEC\text{-}HPS}$ = −12.13 ‰.

For Li, we processed and measured an in-house standard of aragonite sand (ARAG) and seawater. The long term reproducibility for these standards are δ^7Li_{ARAG}= +20.1 ± 1.2 ‰ (2σ, n = 21) and δ^7Li_{SW}= +31.6 ± 1.5 ‰ (2σ, n = 92), respectively. Our measured δ^7Li_{sw} value is indistinguishable from published values (Supplementary Material). ARAG standard values and three modern aragonitic corals standards, ERP (δ^7Li_{ERP}= +19.6 ± 1.5 ‰, 2σ, n = 14), JCP-1 ($\delta^7Li_{JCP\text{-}1}$= +18.9 ± 1.5 ‰, 2σ, n = 3), and JCP-1B ($\delta^7Li_{JCP\text{-}1B}$= +19.9 ± 1.1 ‰, 2σ, n = 7) are consistent with an experimentally and empirically determined fractionation factor for aragonite of $\Delta^7Li_{Arag\text{-}SW} \simeq -12$ ‰ (Marriott et al., 2004a,b; Rollion-Bard et al., 2009; Gabitov et al., 2011; Bastian et al., 2018; Bohlin et al., 2018; Dellinger et al., 2018; Taylor et al., 2019; Day et al., 2021). We therefore consider the external precision of our lithium isotope measurements to be ± 1.5 ‰ (2σ).

3.5. Other geochemical and mineralogical data

We pair measurements of δ^7Li values with a large dataset of sediment mineralogy, δ^{13}C, δ^{18}O, δ^{44}Ca, δ^{26}Mg, and elemental concentration from previous studies of the same samples, though not the same leachates (Vahrenkamp et al., 1988; Eberli et al., 1997; Feary et al., 2000; Melim et al., 2001; Higgins et al., 2018). We also include previously published data from ODP Site 1007 on the toe of the GBB slope (Eberli et al., 1997; Higgins et al., 2018; Dellinger et al., 2020) and from Bahamas bank top sediment (Swart et al.,

2009; Zhang et al., 2017; Higgins et al., 2018; Pogge von Strandmann et al., 2019).

3.6. Numerical model of diagenesis

To quantitatively examine the influence of diagenesis on the geochemical variability of bulk carbonate sediments, we apply a numerical mass-balance model of early marine carbonate diagenesis and dolomitization (Fig S1; model was adapted from Ahm et al., 2018. Please refer therein for detailed description of model construction and to the supplement of this paper for model parameters). The model simulates advection along a one-dimensional path through permeable carbonate sediment in which primary calcium carbonate is dissolved and a secondary carbonate phase (dolomite or LMC) is precipitated at a prescribed reaction rate. The model flow path is divided into a sequence of discrete boxes (box 1 to box N), each representing a volume of porous sediment in which carbonate dissolution/precipitation reactions occur (Fig. S1). The chemical composition of the fluid evolves along the flow path following a fluid-buffered (box 1) to sediment-buffered (box N) trajectory, and we track the chemistry of the fluid and bulk carbonate (Fig. 3). Where a carbonate mineral phase is dissolved and reprecipitated as the same polymorph, we use the term *recrystallization* (Sorby, 1879; Dixon and Vaughan, 1911). The term *neomorphism* is reserved for the conversion of one calcium carbonate phase to another (e.g. aragonite to LMC) and the term *dolomitization* is used where calcium carbonate is converted to dolomite ($CaMg[CO_3]_2$) (Folk, 1965). Diagenetic alteration (recrystallization, neomorphism, and dolomitization) are modeled as stoichiometric assuming conservation of mass of carbon in the sediment (i.e., no net dissolution or precipitation, an assumption supported by pore fluid evidence from the same Bahamian cores, Higgins et al., 2018).

The terms "fluid-buffered" and "sediment-buffered" are defined with respect to a particular elemental or isotopic system. Unless otherwise noted, we use "fluid-buffered" and "sediment-buffered" to refer to diagenetic conditions with respect to calcium in the sediment as it, together with carbon, tends to be the most diagenetically robust geochemical proxy in carbonate sediments. Although we use the conversion of Bahamian surface sediment to dolomite to illustrate model behavior, similar sets of calculations were performed for other starting (primary) and ending (diagenetic) carbonate mineralogies, e.g., Site 1131 sediment to LMC. Parameters of these calculations can be found in the supplementary material.

The model results provide quantitative constraints on (1) the composition and mineralogy of the primary carbonate, (2) the composition of the diagenetic carbonate, and (3) the composition of the diagenetic fluid. The model predicts diagnostic pathways in geochemical cross-plot space, ranging from sediment-buffered to fluid-buffered conditions, but does not attempt to capture all complexity of the geometry of fluid flow.

The modelled phase-space within geochemical cross-plots are defined by three end-members: (1) the primary (i.e., initial) sediment, (2) the fluid-buffered diagenetic end-member, and (3) the sediment-buffered diagenetic end-member (e.g., Fig. 4). Samples that are fully altered (100 % = all initial carbonate has been transformed to diagenetic carbonate) fall along a mixing line between the fluid-buffered (Box 1) and sediment-buffered (Box N) end members. Bulk samples that plot between the primary sediment and the fully altered mixing line (between 0 and 100 %) are interpreted to be partially altered under the modeled diagenetic conditions. The effects of multiple diagenetic events under different conditions (e.g., later marine or meteoric diagenesis) can be explored by running the model again with a new parameter-set (fluid composition, flow rate, etc.) and using an average sediment composition from previous model results as the new initial sediment composition.

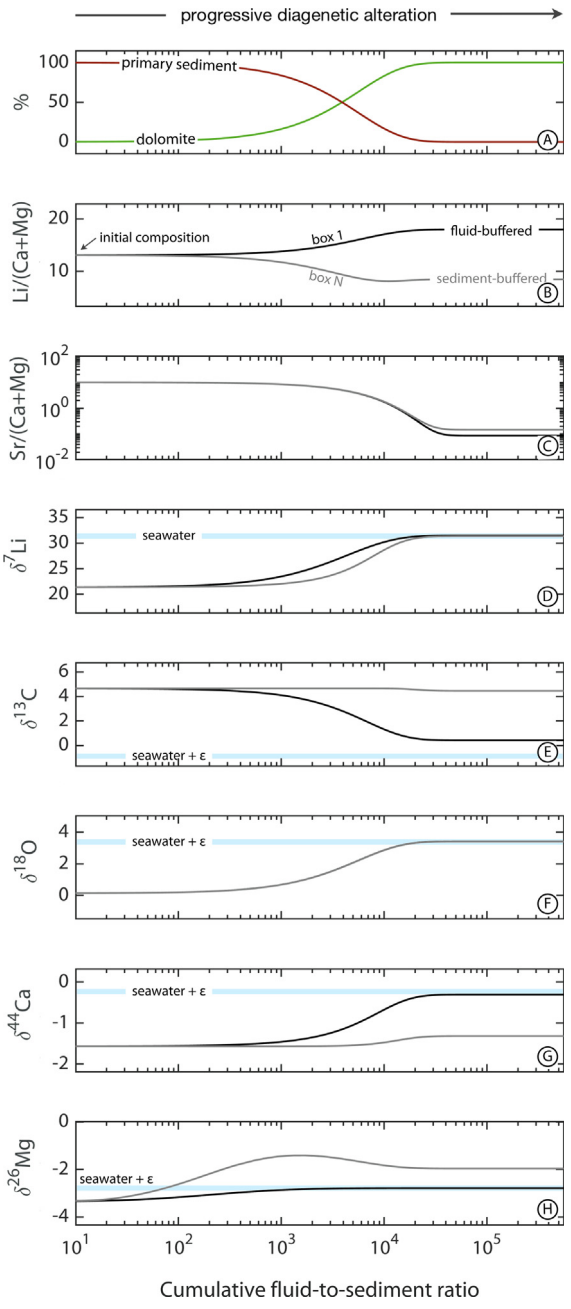

Fig. 3. Model results for change in bulk sediment chemistry during diagenesis of primary Bahamian sediment (93 % aragonite, 7 % HMC) to dolomite $(Ca,Mg)(CO_3)_2$ with modern seawater. The composition of the bulk sediment evolves as fluid flows through the sediment at a constant advection rate (i.e., increasing cumulative mass of fluid relative to the sediment over time). The specific geochemical trajectory depends on the length of the flow path (i.e., the specific box number), where box 1 (black) represents the fluid-buffered endmember and box N (grey) is the most sediment-buffered with respect to calcium. (A) Percentage of bulk sediment that is extant primary sediment and diagenetic dolomite during progressive alteration of Bahamian sediment to dolomite at a prescribed reaction and advection rate. (B) Changes in bulk sediment Li/(Ca + Mg) ratios (μmol/mol). (C) Changes in bulk sediment Sr/(Ca + Mg) ratios (mmol/mol). (D) Changes in bulk sediment δ^7Li values (‰). (E) Change in bulk sediment δ^{13}C values (‰). (F) Change in bulk sediment δ^{18}O values (‰). (G) Change in bulk sediment $\delta^{44/40}$Ca values (‰). (H) Change in bulk sediment δ^{26}Mg values (‰).

3.7. Model Inputs

Model input parameters, which are derived from previous experimental and empirical work (Ahm et al., 2018 Table 1 and references therein) and new data presented here, include (1)

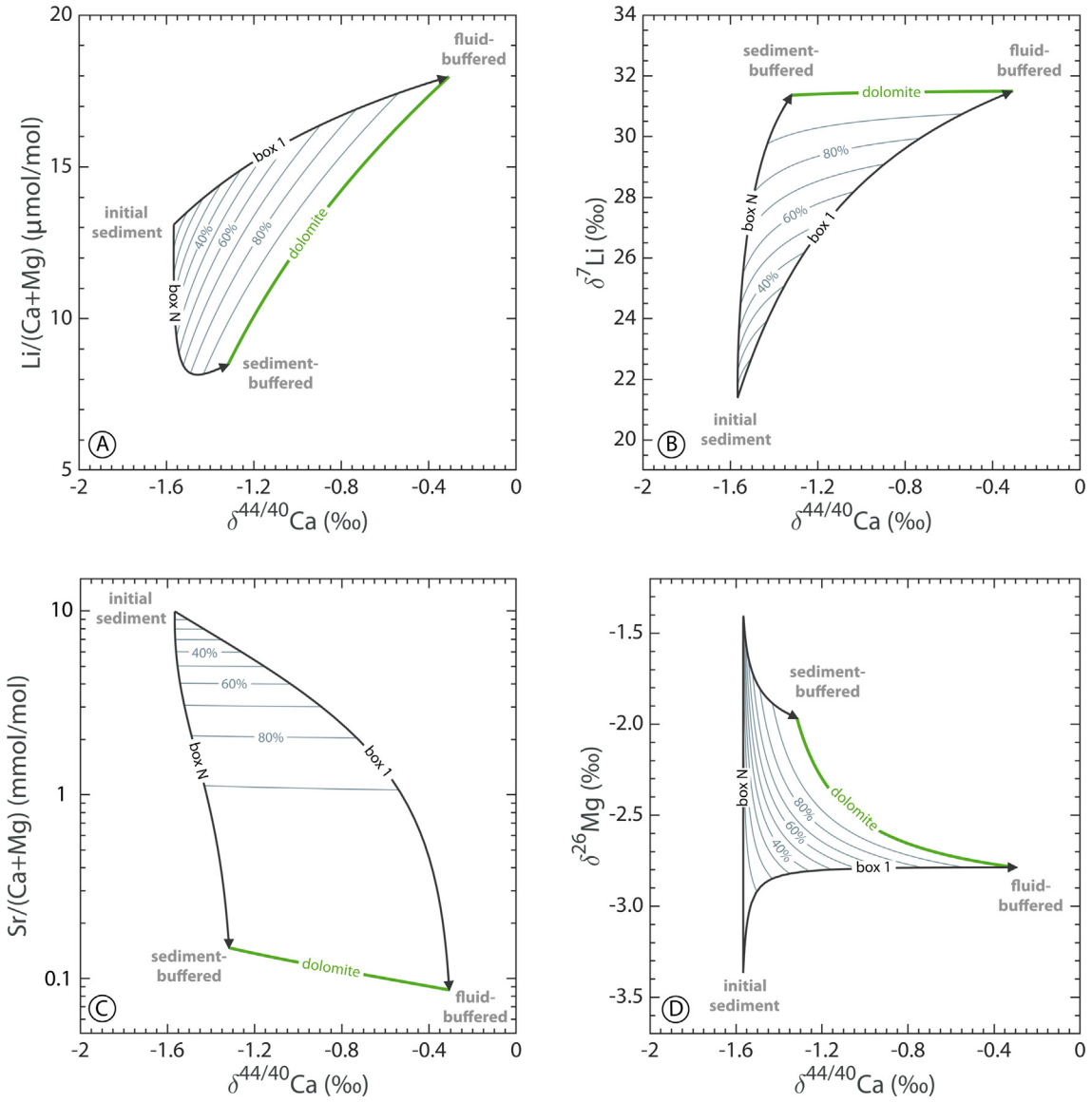

Fig. 4. Geochemical cross-plots of model results showing the range of bulk sediment compositions that can be explained by dolomitization of primary Bahamian sediment (93 % aragonite, 7 % HMC) by modern seawater. Gray lines represent the percent (0 % to 100 %) of primary sediment that has been altered. The range in compositions of fully dolomitized sediment is represented by the diagenetic endmember (thick green line). The modelled geochemical pathways for a fluid- and sediment-buffered endmember during dolomitization is defined by the box 1 and box N trajectories, respectively. (A). Modeled trajectories illustrating the correlation between Li/(Ca + Mg) ratios and $\delta^{44/40}$Ca values in the bulk sediment during dolomitization. (B) Modeled trajectories illustrating the correlation between δ^7Li and $\delta^{44/40}$Ca values in the bulk sediment during dolomitization. For fully dolomitized sediment, despite the system being fully sediment-buffered (with respect to Ca) in box N, the δ^7Li value is consistently reset across all boxes. (C) Modeled trajectories illustrating the correlation between Sr/(Ca + Mg) ratios and $\delta^{44/40}$Ca values in the bulk sediment during dolomitization. (D) Modeled trajectories illustrating the correlation between δ^{26}Mg and $\delta^{44/40}$Ca values in the bulk sediment during dolomitization. (For interpretation of the references to colour in this figure legend, the reader is referred to the web version of this article.)

advection and reaction rates, (2) the elemental and isotopic composition of the primary sediment, (3) the elemental and isotopic composition of the diagenetic fluid, (4) the distribution coefficients and (5) isotopic fractionation factors for the diagenetic mineral (supplementary material).

The lithium elemental and isotopic composition of bulk marine carbonate sediment depends on mineralogy. Considering carbonate minerals precipitated from modern seawater, both experimental and empirical evidence from modern carbonate environments support an estimated average aragonite composition of Li/(Ca + Mg) ≈ 9 µmol/mol (Marriott et al., 2004a,b; Hathorne et al., 2013; Zhang et al., 2017; Dellinger et al., 2018; Dellinger et al., 2020) and δ^7Li ≈ 20 ‰ (Marriott et al., 2004a,b; Rollion-Bard et al., 2009; Bastian et al., 2018; Bohlin et al., 2018; Taylor et al., 2019; Pogge von Strandmann et al., 2019). HMC has been shown to have significantly higher lithium content (Li/(Ca + Mg) ~ 60 µmol/mol) and higher δ^7Li values (~24 ‰), relative to aragonite (Dellinger et al., 2018). Biogenic and inorganic LMC typically has Li/(Ca + Mg) ~ 10–20 µmol/mol, depending of physiochemical fluid conditions during carbonate precipitation (Marriott et al., 2004a,b; Hall and Chan, 2004; Hall et al., 2005; Hathorne and James, 2006; Misra and Froelich, 2012; Füger et al., 2019;) and δ^7Li ~ 25–30 ‰ (Marriott et al., 2004a,b; Hathorne and James, 2006; Rollion-Bard et al., 2009; Misra and Froelich, 2012; Pogge von Strandmann et al., 2019; Day et al., 2021). We assume a composition of primary LMC of Li/(Ca + Mg) = 18 µmol/mol and δ^7Li = 29 ‰.

The mineralogy of Bahamian primary sediment used in the model is 93 % aragonite and 7 % HMC (Reijmer et al., 2009) resulting in a bulk composition of Li/(Ca + Mg) ~ 13 µmol/mol and

δ^7Li = 20 ‰. At Site 1131, the mineralogy of the top 60 cm of the core has a significant portion of HMC (60 %), and equal parts aragonite and LMC (20 % each) (Feary et al., 2000). Based on simple mixing calculation, we assume bulk surface sediment at Site 1131 to have Li/(Ca + Mg) = 39 μmol/mol and δ^7Li = 24 ‰. Primary fluid entering the sediment at all sites is assumed to be unaltered seawater with a composition of Li/Ca = 2500 μmol/mol and δ^7Li = 31.5 ‰. Distribution coefficients and fractionation factors for lithium into diagenetic minerals (e.g., LMC and dolomite) are not independently known from experimental work and are estimated here by fitting the model to the data. Estimated distribution coefficients are K_D^{Li} = 0.003 and K_D^{Li} = 0.008 for diagenetic LMC and dolomite, respectively, while fractionation factors are estimated at α= ~1.000 for both diagenetic minerals.

4. Results

4.1. Modern Samples

4.1.1. Seawater survey

Measured δ^7Li_{sw} values (supplemental material) are uniform at all sites (31.58 +/− 0.7 ‰, n = 32) and show no trend with latitude, longitude, or depth below sea surface. The mean value matches the long-term mean of our in-house seawater standard (31.57 +/− 0.08 ‰, 2SE, n = 92) and is consistent with published values (Reference list provided in supplementary material).

4.1.2. Bahamas Surface Sediment

Measured Bahamian surface sediment δ^7Li values and Li/(Ca + Mg) ratios are 18.7 ± 2.9 ‰ and 14.1 ± 6.3 μmol/mol (n = 11), respectively (supplementary material). However, carbonate mud samples from Triple Goose Creek (TGC) have elevated lithium, aluminum, and magnesium content suggesting some minor leaching of lithium from silicate minerals during sample digestion. Correlations of δ^7Li, Li/(Ca + Mg), and Al/(Ca + Mg) in Fig. S2 imply a carbonate end-member composition of δ^7Li = 20.6 ± 0.5 ‰ and Li/(Ca + Mg) = 8.6 ± 0.7 μmol/mol for TGC surface sediment. These values are consistent with the expected value for aragonite precipitated from modern seawater with a fractionation of $\Delta^7Li_{arag\text{-}sw}$ ~ −12 ‰ and distribution coefficients of K_D^{Li} ~ 0.003 (Marriott et al., 2004b), as well as published values for Bahamas surface sediment (Zhang et al., 2017; Pogge von Strandmann et al., 2019).

Measured $\delta^{44/40}$Ca values for surface sediment samples from the Bahamas ($\delta^{44/40}$Ca = −1.54 +/− 0.24 ‰, n = 11) are consistent with a fractionation factor ($\alpha^{44/40}$ ~ 0.9985, Gussone et al., 2005) for inorganic aragonite from seawater ($\delta^{44/40}Ca_{SW}$ = 0 ‰) and previously reported values from the Bahamas ($\delta^{44/40}$Ca = −1.36 +/− 0.16 ‰, n = 17) (Higgins et al., 2018).

4.2. Bahamas Core Samples

4.2.1. Li/(Ca + Mg) ratios

Measured Li/(Ca + Mg) ratios of all Bahamian core samples are 13.0 +/− 8.2 μmol/mol (n = 281). In general, the lithium content is not correlated with δ^7Li values or other elemental and isotopic systems (Figs. 2 & 5). The average value for dolomite samples (14.6 ± 6.1 μmol/mol, n = 84) is slightly higher than the overall average, but otherwise lithium content is not correlated with bulk sediment mineralogy. Sediment below major hardgrounds and/or erosional surfaces at Clino (367 mbsf and 536 mbsf) and Unda (~110 mbsf) show Li/(Ca + Mg) ratio profiles that extend over ~ 50 m with elevated values (~20 μmol/mol) at the surface that decrease with depth to a background value similar to bank top sediment (~8 μmol/mol).

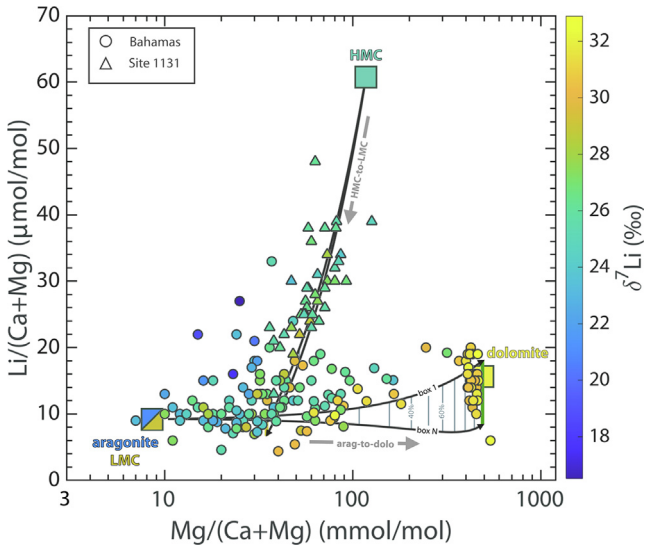

Fig. 5. Covariation between bulk sediment Li/(Ca + Mg) and Mg/(Ca + Mg) ratios at Bahamas sites and Site 1131 with model results for the diagenetic transformation of HMC-to-LMC and aragonite-to-dolomite by modern seawater. Boxes are representative values for pure carbonate minerals. Samples are colored by measured δ^7Li values; boxes are colored by representative δ^7Li values. A strong correlation between Li/(Ca + Mg) and Mg/(Ca + Mg) ratios is unique to altered sediment of predominantly LMC mineralogy from Site 1131 where primary sediment is predominantly HMC.

Measured Li/(Ca + Mg) ratios at Site 1131 (27.4 +/− 12.2 μmol/mol, n = 74) are higher and have greater variability than all Bahamian sites (Fig. 2). The mean ratio decreases with depth within the top 100 m of the core in concert with a decrease in proportions of HMC, but then remains generally invariant and elevated (~26 μmol/mol) throughout the rest of the core where bulk sample mineralogy is predominantly LMC. For comparison, lithium content is twice that of Bahamas core samples that have predominantly LMC mineralogy (~13 μmol/mol).

4.2.2. Lithium Isotopes

Across all Bahamian sites, the range of δ^7Li values falls between the inferred δ^7Li value of Miocene to modern seawater (26–31 ‰, Misra and Froelich, 2012) and the expected δ^7Li value of Miocene to modern aragonite (14–19 ‰, based on a fractionation factor of $\Delta^7Li_{arag\text{-}sw}$ ~ -12 ‰). Within this range, δ^7Li values are correlated with bulk carbonate mineralogy and geochemistry (Fig. 2). Samples having significant proportion of aragonite (e.g., above 243 mbsf at Site 1003 and between 150 and 366 mbsf in Clino) are characterized by low δ^7Li and $\delta^{44/40}$Ca values and elevated Sr/(Ca + Mg) ratios. In contrast, samples having a significant proportion of dolomite (e.g., ~200mbsf at Site 1003, below 540 mbsf at Clino, and all measured samples from Sites Unda, San Salvador, and LBB) are characterized by elevated δ^7Li values equal to contemporaneous seawater (~31 ‰), elevated $\delta^{44/40}$Ca values (~-0.5 ‰), and very low Sr/(Ca + Mg) ratios (~200 μmol/mol). Sections that contain predominately LMC mineralogy (e.g., below 200mbsf at Site 1003, below 367 mbsf at Clino) have δ^7Li values spanning ~ 15 ‰, a range greater than secular change in Cenozoic seawater inferred from foraminifera (~9‰, Hathorne and James, 2006; Misra and Froelich, 2009). For instance, within the lower 130 m of Site 1003, δ^7Li values span 10 ‰ between values equal to Early Miocene seawater (δ^7Li ~ 26 ‰; Misra and Froelich, 2012) and aragonite precipitated from Early Miocene seawater (δ^7Li ~ 16 ‰). Additionally, the predominately LMC sections include stratigraphic trends not associated with mineralogy or secular changes in the δ^7Li value of contemporaneous seawater. For examples, at Site 1003 between 700 and 900 mbsf, δ^7Li values

show a coherent 5 ‰ negative excursion. Within these LMC sections δ^7Li values are moderately correlated with $\delta^{44/40}$Ca values and anti-correlated with Sr/(Ca + Mg) ratios.

Samples from Site 1131 are characterized by generally uniform δ^7Li values (26.1 +/− 2.5 ‰, n = 39) with an average offset from contemporaneous seawater of ~ 5 ‰, along with uniform $\delta^{44/40}$Ca values near −1.0 ‰ and Sr/(Ca + Mg) ratios of 3300 μmol/mmol. Though subtle, some stratigraphically coherent trends are apparent. Lithium isotope values increase downcore from 26 ‰ at the top of the core up to 29 ‰ at depth 100 mbsf in concert with decreasing percentage of HMC. Below this depth, δ^7Li values oscillate between 24 ‰ and 27 ‰ and are positively correlated with $\delta^{44/40}$Ca values (r^2 = 0.55), but independent of mineralogy.

4.3. Diagenetic model

Model results for Li/(Ca + Mg) ratios and δ^7Li values, together with other carbonate-bound geochemical proxies, can be understood in terms of how the evolution of fluid chemistry along a flow path results in changes in the chemical composition of diagenetic minerals precipitated along that flow path (Fig. 3). At locations closest to the fluid source (Box 1) the chemistry of pore-fluid resembles that of the source fluid and diagenetic minerals that precipitate from this fluid will have a composition that is determined by the source fluid (fluid-buffered). In contrast, further along the flow path pore-fluid composition is increasingly dominated by recrystallization, neomorphism, or dolomitization of carbonate sediment earlier along the flow path until the composition of the pore-fluid has evolved to the point (e.g., Box N) where the diagenetic minerals that precipitate from this fluid are similar in chemical and isotopic composition to the initial sediment (sediment-buffered). Both Box 1 and Box N will have experienced the same cumulative fluid-to-sediment ratio (i.e., will have 'seen' the same volume of diagenetic fluid) and have undergone the same extent of alteration, but the elemental and isotopic composition of the diagenetic minerals in the two boxes will differ as a result of the chemical evolution of the pore fluid along the flow path.

Fluid-buffered diagenetic conversion of Bahamian sediment to dolomite (Box 1) exhibits a synchronous change in all geochemical proxies, including Li/(Ca + Mg) and δ^7Li values (Fig. 3). The bulk geochemistry, in this case, results from simple endmember mixing of diagenetic dolomite minerals precipitated from unaltered seawater with extant primary sediment. In this scenario, the geochemistry of the diagenetic mineral is controlled by the composition of seawater and the relevant partition coefficients and isotopic fractions factors. Once all of the precursor carbonate (e.g., predominantly aragonite) has been altered to diagenetic minerals (e.g., dolomite), the bulk geochemistry will reflect the composition of the diagenetic fluid (e.g., seawater) modulated by the relevant fractionation factors and distribution coefficients. Since Li isotopic fractionation factors and partition coefficients under diagenetic conditions are not well constrained from laboratory experiments, we estimate these parameters empirically by fitting the model to our data. In our most altered samples (dolomite, model Box 1), Li/(Ca + Mg) ratios and δ^7Li values both increase, reflecting a prescribed higher partition coefficient for Li/(Ca + Mg) in dolomite ($K_D^{Li\text{-}dolo} \sim 0.008$ vs $K_D^{Li\text{-}arag} \sim 0.003$) and a much smaller fractionation factor ($\Delta^7Li_{dolo\text{-}sw}$ = 0 ‰ vs $\Delta^7Li_{arag\text{-}sw}$ = −12 ‰) compared to aragonite.

In contrast to the fluid-buffered endmember (Box 1), the chemical composition of the sediment-buffered endmember, modeled by the farthest box along the flow-path (Box N), depends on the isotope effects and/or partition coefficients associated with a particular chemical system. For example, both δ^{13}C and $\delta^{44/40}$Ca values of box N are shifted only slightly from the initial sediment composition, a result of the high concentration of carbon and calcium in carbonate sediments. In contrast, δ^{18}O values in Box N remain indistinguishable from values in Box 1, signifying that oxygen isotopes are fluid-buffered over the entire modelled flow path. Similar to δ^{18}O, bulk sediment δ^7Li values are uniform in all boxes and directly records the δ^7Li value of seawater (Fig. 3, estimated fractionation factor of α = 1.000).

Model results also demonstrate that during dolomitization, Li/(Ca + Mg) ratios can either be elevated or depleted relative to the initial sediment (Fig. 3B). In the fluid-buffered dolomite endmember (Box 1), Li/(Ca + Mg) values are elevated relative to aragonite due to a higher partitioning of Li into dolomites. As a result of the higher uptake of lithium into dolomites relative to aragonite, pore fluids further along the flow-path are depleted of Li and sediment-buffered dolomites precipitated from the Li-depleted pore fluid (e.g., Box N) have commensurately lower Li/(Ca + Mg) values.

4.3.1. Geochemical Cross-plots

Since past fluid flow and diagenetic reaction rates are poorly constrained for sedimentary carbonates in the geologic record, the utility of our diagenetic model lies in its ability to explain covariation between multiple sets of geochemical data (i.e., δ^{13}C, δ^{18}O, $\delta^{44/40}$Ca, δ^{26}Mg, Sr/(Ca + Mg) ratios) (Fig. 4). As diagenetic alteration proceeds in time (i.e., % initial sediment altered increases), each box in the model will carve out a diagnostic trajectory in cross-plots of carbonate-bound geochemical proxies (e.g., δ^7Li vs $\delta^{44/40}$Ca) with the shape of each trajectory being determined by extent to which the diagenetic conditions in the box reflect fluid- or sediment-buffered conditions for the specific proxy during alteration. For each set of geochemical proxies, the area bounded by the model trajectories for the fully fluid-buffered box (1) and the most sediment-buffered box (N) represents the model space that can be explained by early marine diagenesis. Inherent in this approach is the assumption that the boundary conditions (e.g., seawater composition, primary sediment composition, pore fluid physiochemical conditions) remain constant during early marine diagenesis. Interpreted in this way the data and model boundary conditions provide a single snapshot of the chemical composition of the ocean in the geologic past.

4.3.1.1. Sr/(Ca + Mg) vs $\delta^{44/40}$Ca. As Sr/(Ca + Mg) ratios and $\delta^{44/40}$Ca values are controlled by both mineralogy (e.g., aragonite vs calcite) and early marine diagenesis, cross plots of these variables provide a framework for evaluating the influence of mineralogy and style of diagenetic alteration on bulk carbonate chemistry (Higgins et al., 2018; Ahm et al., 2018). In marine diagenetic settings calcium isotopes are relatively resistant to alteration due to high concentrations of Ca in carbonate sediment relative to marine fluid. Model results show the sediment buffered endmember largely retains primary $\delta^{44/40}$Ca values composition of the initial sediment whereas the fluid-buffered endmember is altered toward higher values. Among carbonate minerals, aragonite is uniquely characterized by elevated Sr content (Sr/Ca ~ 10 mmol/mol; Odum, 1950; Lowenstam 1961; Kinsman, 1969), while diagenetic carbonate minerals (calcite and dolomite) are characterized by much lower Sr content (<1 mmol/mol; Kinsman, 1969; Banner, 1995). Progressive alteration of aragonite to dolomite under fluid-buffered conditions will therefore be associated with a lowering of sediment Sr/(Ca + Mg) ratio and increasing in $\delta^{44/40}$Ca values (Box 1 trajectory). Under sediment-buffered conditions (Box N trajectory), our model predicts that due to the accumulation of Sr in pore fluids along the flow path, the decline in sediment Sr/(Ca + Mg) will be less than under fluid-buffered conditions while $\delta^{44/40}$Ca values will remain similar to the initial sediment (Fig. 4c).

4.3.1.2. Li/(Ca + Mg) vs $\delta^{44/40}$Ca. In contrast to the covariation of Sr/(Ca + Mg) ratio and $\delta^{44/40}$Ca values under both fluid- and sediment-buffered conditions, model results indicated that the effects of mineralogy and diagenesis on Li/(Ca + Mg) are more subtle and can both increase and decrease Li content in sediment depending on the conditions of alteration and mineralogy (calcite vs dolomite) of the diagenetic minerals (Fig. 4a). The fluid-buffered endmember follows a trajectory of positive covariation of Li/(Ca + Mg) and $\delta^{44/40}$Ca, which can be explained by simple mixing of extant primary sediment with diagenetic minerals with elevated $\delta^{44/40}$Ca and Li/(Ca + Mg) due to the higher partitioning coefficient of dolomite relative to aragonite used in the model. The sediment buffered endmember follows a trajectory of decreasing Li/(Ca + Mg) with increasing $\delta^{44/40}$Ca due to a depletion of Li in the pore fluid along the flow path. This behavior results in fully altered sediment with lithium content ranging both greater than and less than the primary sediment, and a positive covariation in Li/(Ca + Mg) and $\delta^{44/40}$Ca values.

4.3.1.3. δ^7Li vs $\delta^{44/40}$Ca. Cross plots of δ^7Li vs $\delta^{44/40}$Ca values show covariation when a fraction of the bulk sediment has been dolomitized (alteration < 100 %) and no covariation in the fully diagenetic end-member (100 % altered) (Fig. 4b). This result indicates that under the conditions modelled lithium in the diagenetic mineral is fluid-buffered over the entire diagenetic length scale (over all modelled boxes). Increasing the length scale, increasing the reaction rate (R), or decreasing the rate of fluid flow (u), or any combination of the three can produce model results with more sediment-buffered conditions for lithium isotopes in the fully altered endmember. In any scenario where diagenetic mineral δ^7Li values fall between that of the initial sediment (sediment-buffered with respect to Li) and seawater (fluid-buffered with respect to Li), $\delta^{44/40}$Ca values will be sediment buffered due to calcium's much higher concentration in sediment relative to marine-derived diagenetic fluids (Fig. 4B; see also Fig. 3B in Dellinger et al., 2020). Therefore, evidence of fully sediment-buffered conditions with respect to $\delta^{44/40}$Ca does not provide indication as to whether δ^7Li values are sediment- or fluid-buffered. However, any diagenetic context that produces less than fully sediment-buffered conditions with respect to $\delta^{44/40}$Ca values will yield fully fluid-buffered δ^7Li values in the same diagenetic minerals. For samples that have not been fully recrystallized during early marine diagenesis (alteration < 100 %), mixtures of extant initial sediment with fully fluid-buffered (with regards to Li) minerals can produce bulk sediment δ^7Li values that are intermediate between that of the initial sediment and diagenetic minerals.

5. Discussion

The lithium isotopic composition of marine carbonate rocks depends on (1) the isotopic composition of seawater at the time of primary precipitation, (2) the carbonate mineralogy (e.g., aragonite vs calcite) and associated isotope fractions, and (3) the full diagenetic history of the rock. Our data, which span a wide range of water depths and marine diagenetic environments, exhibits large (up to 10 ‰) stratigraphic changes in bulk sediment δ^7Li values that are unrelated to changes in the δ^7Li value of seawater. Instead, the variations in bulk sediment δ^7Li values can be explained by variations in mineralogy and/or diagenesis, suggesting that these processes exert a primary control on the δ^7Li value of bulk shallow-water marine carbonates in the geologic record. However, pairing measurements of bulk sediment δ^7Li values with independent geochemical indicators of mineralogy and diagenesis – $\delta^{44/40}$Ca values, δ^{26}Mg values, and trace element ratios – provides a path to extracting 'snapshots' of seawater δ^7Li values and reconstructing the δ^7Li of seawater throughout Earth history.

5.1. Mineralogy

The mineralogy of the primary carbonate precipitate plays a key role in the stratigraphic variability of bulk carbonate Li/(Ca + Mg) ratios and δ^7Li values through differences in the distribution coefficients and isotopic fractionation factor (Marriott et al., 2004a,b; Dellinger et al., 2018). This is observed throughout our dataset as both Li/(Ca + Mg) ratios and δ^7Li values are correlated with abundance of aragonite and HMC (Fig. 5).

For example, in the upper 200 m of Sites 1007 and 1003, a decrease in aragonite content is correlated with an increase in δ^7Li and $\delta^{44/40}$Ca values and a decrease in Sr content (Fig. 2). Similar covariations are observed between 150 and 366 mbsf in the Clino core, where aragonite abundance is positively correlated with Sr content and anti-correlated with δ^7Li and $\delta^{44/40}$Ca values. These trends result from aragonite minerals having the most elevated strontium content and the largest magnitude fractionation of lithium and calcium isotopes ($\Delta^7Li_{fluid\text{-}arag} \sim 12$ ‰ and $\Delta^{44/40}Ca_{fluid\text{-}arag} \sim 1.5$ ‰) relative to other carbonate minerals (Marriott et al., 2004a,b; Dellinger et al., 2018). In contrast to δ^7Li values, bulk sediment Li/(Ca + Mg) ratios are uniform with depth in these sections, suggesting aragonite and diagenetic low-Mg calcite have similar distribution coefficients in these types of settings, or that any difference in partition coefficients due to mineralogy is overwhelmed by other factors (e.g., temperature, salinity, precipitation rate, etc.).

The role of HMC in determining bulk sediment δ^7Li values and Li/(Ca + Mg) ratios is best illustrated at Site 1131 (Fig. 2). The upper 70 m of Site 1131 shows decreasing HMC abundance with depth associated with increasing δ^7Li values and decreasing Li content, trends that are consistent with empirical studies of Li isotope fractionation ($\Delta^7Li_{fluid\text{-}HMC} \sim 6$ ‰) and Li/(Ca + Mg) ratios (~80 μmol/mol) of HMC (Darrenougue et al., 2014; Dellinger et al., 2018). Because HMC is characterized by intermediate and non-unique δ^7Li values, $\delta^{44/40}$Ca values, and Sr/(Ca + Mg) ratios relative to aragonite and LMC, differentiating the influence of constituent HMC minerals on bulk geochemistry from mixtures of aragonite and diagenetic LMC is best accomplished through a cross-plot of Li/(Ca + Mg) vs Mg/(Ca + Mg) ratios (Fig. 5). Since HMC is uniquely characterized among calcium carbonate minerals by significantly elevated Li and Mg content, positive covariations of Li/(Ca + Mg) and Mg/(Ca + Mg) ratios indicate the influence of constituent HMC on bulk sediment geochemistry.

The effects of mineralogy on the δ^7Li value of LMC and dolomite is more difficult to determine from our dataset as these minerals are largely diagenetic in origin and therefore any mineralogical influence is convolved with the effects of diagenesis. As a result, the δ^7Li value and Li/(Ca + Mg) ratio of LMC and dolomite may span a ~ 12 ‰ and 10x range, respectively, depending on the extent to which diagenesis occurred under fluid- or sediment-buffered conditions with respect to Li, discussed in the following section.

5.2. Early marine Diagenesis

Samples from the Bahamas exhibit a wide range of diagenetic conditions. Perhaps the most striking feature of our data is that all dolomitized sections (Unda, SS, and LBB) are characterized by δ^7Li values (31.1 ± 1.7 ‰, n = 50) that are both indistinguishable from one another and equal to modern/Late Neogene seawater (31.5 ‰). This result, when considered in the context of the extensive body of geochemical data from these same Bahamian cores (Table 1 in Murray et al., 2021; Dellinger et al., 2020;

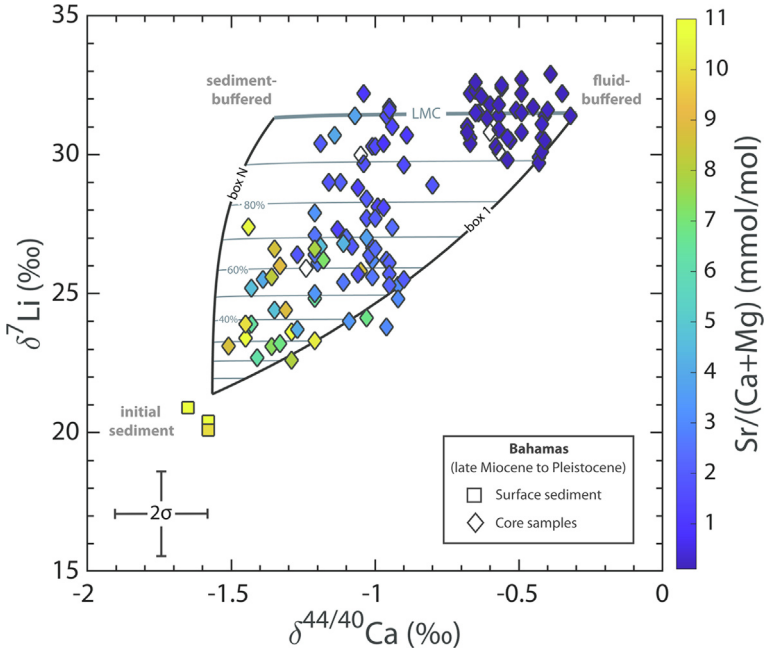

Fig. 6. Model results for neomorphism of Bahamas primary sediment (93 % aragonite, 7 % HMC) by modern seawater with measured surface sediment (free of silicate contamination) and all Bahamian core samples of late-Miocene to Pleistocene age plotted as δ^7Li values vs $\delta^{44/40}$Ca values. Samples are colored by measured Sr/(Ca + Mg) ratios.

Wang et al., 2021), indicates that there is little to no fractionation of Li isotopes during its incorporation into dolomite ($\alpha \sim 1.000$). As a result, under the fluid-buffered conditions that characterize the studied Bahamian dolomites (e.g., $\delta^{44/40}$Ca = −0.8 to −0.3 ‰, Fig. 6), the δ^7Li value of the dolomite directly records the δ^7Li value of seawater.

In contrast to the uniform δ^7Li values and ∼ 2x range in Li/(Ca + Mg) ratios associated with dolomite, in LMC-dominated sections we see stratigraphic trends in δ^7Li values and Li/(Ca + Mg) ratios ranging over 16 ‰ and a factor of ∼ 10x, respectively. Although some of this stratigraphic variability likely reflects contributions from pelagic LMC (Swart, 2008), most of the variability can be explained by early marine diagenesis under a range of fluid- and sediment-buffered conditions (Higgins et al., 2018).

To understand the source of the variability described above, we used paired measurements of $\delta^{44/40}$Ca and δ^{26}Mg values and Sr/(Ca + Mg) ratios as a framework to identify geochemical signals associated with early marine diagenesis and characterize the diagenetic style (i.e., fluid- vs sediment-buffered) (Fantle and Higgins, 2014; Blättler et al., 2015; Higgins et al., 2018; Ahm et al., 2018). This framework can explain both the homogeneous δ^7Li values associated with dolomite and the variability in δ^7Li values associated with LMC in our sample suite.

Diagenetic model results are consistent with the observed covariation in Sr/(Ca + Mg) ratios, $\delta^{44/40}$Ca values, and δ^7Li values in Bahamian bulk samples, supporting the interpretation that diagenesis is the dominant control on the geochemistry of these altered carbonates (Fig. 6). First, samples with δ^7Li values close to the primary sediment endmember (∼20 ‰) are elevated in Sr content and depleted in ^{44}Ca, consistent with incomplete diagenetic recrystallization of aragonite (e.g., the top 150 m of Sites 1007 and 1003, and at Site Clino between 150 and 364 mbsf). Second, the model also captures bulk sediment with δ^7Li values that are moderately sediment-buffered with respect to lithium and characterized by low $\delta^{44/40}$Ca values and intermediate Sr/(Ca + Mg) ratios (e.g., 793, 1181, and 1293 mbsf at Site 1003 and 379 mbsf at Site Clino, Figs. 2 & 6). Third, the model reproduces the bulk chemical and isotopic compositions associated with fluid-buffered diagenetic conditions; bulk samples with δ^7Li values at or near modern seawater (31.5 ‰) are dramatically depleted in Sr and enriched in ^{44}Ca, approaching $\delta^{44/40}$Ca values expected for diagenetic calcite in equilibrium with seawater ($\delta^{44/40}$Ca ∼ -0.2 ‰, Mills et al., 2021). In addition, measured dolomite samples are characterized by uniform and low δ^{26}Mg values (supplementary material) that are consistent with the observation of uniform δ^7Li values and the interpretation that dolomitization occurred under fluid-buffered conditions (Fig. 4d, e.g., Unda, SS, and LBB, at Sites 1003 and 1007 around 250 mbsf, and at Site Clino between 150 and 200 mbsf and below ∼ 540 mbsf).

The clearest example of sediment-buffered alteration with respect to lithium is from Site 1131, where predominantly altered sediment retains primary δ^7Li values (Fig. 7). At this site we observe the complete loss of HMC with depth, but little change

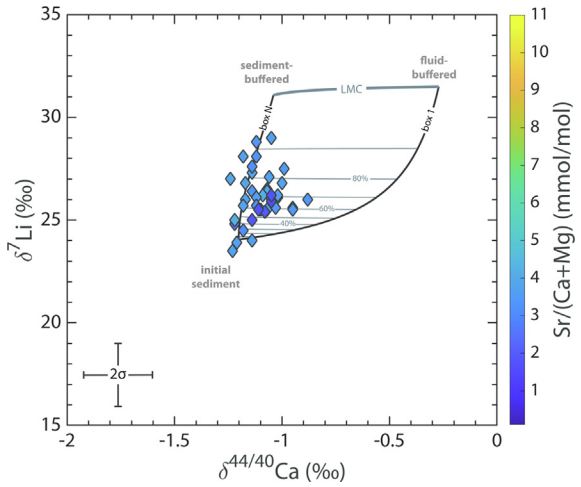

Fig. 7. Model results for the neomorphism of Site 1131 primary sediment (60 % HMC, 20 % aragonite, 20 % LMC) to diagenetic LMC by modern seawater, with measured core samples from Site 1131 plotted as δ^7Li vs $\delta^{44/40}$Ca values. Samples are colored by measured Sr/(Ca + Mg) ratios.

in bulk sediment δ^7Li values. Site 1131 has experienced rapid sedimentation limiting the extent of sediment-fluid interaction and producing sediment-buffered diagenetic conditions throughout (Feary et al., 2000). Model results for this site reproduce the data using a primary sediment composition of 60 % HMC, 20 % aragonite, and 20 % LMC (similar to core-top data). Fig. 7 shows that most samples from Site 1131 fall along a sediment-buffered trajectory, indicating that diagenesis here occurs under conditions of very low advection rates or diffusion-dominated transport of lithium in the pore-fluid. A closed-system interpretation of diagenesis is supported by the observations of dominantly diagenetic LMC mineralogy with low $\delta^{44/40}$Ca values (<-1.0 ‰), elevated Sr/(Ca + Mg) ratios (~3300 mmol/mol), and elevated Li/(Ca + Mg) ratios (27 μmol/mol) throughout of the core. While effectively no HMC minerals remain in the bulk sediment below ~ 70 m, bulk samples have strongly correlated Li/(Ca + Mg) and Mg/(Ca + Mg) ratios that fall on a mixing line between HMC and LMC, suggesting that HMC was indeed a major constituent of the primary sediment (Fig. 5). As expected, lithium isotope values in these predominately sediment-buffered samples (26.1 ± 2.5 ‰, 2σ) generally retain the signature of a predominantly HMC precursor (δ^7Li ~ 24 ‰).

A notable stratigraphic expression of variable styles of early marine diagenesis can be seen in the hardgrounds and underlying sediments at 567 mbsf in Clino and 915 mbsf at Site 1003. Samples from at or near the hardgrounds show geochemical evidence of fluid buffered diagenesis (elevated $\delta^{44/40}$Ca, depleted Sr, and seawater-like δ^7Li) whereas below each hardground these geochemical proxies show a transition to more sediment-buffered conditions (Murray et al., 2021). These features suggest that well defined hardgrounds may serve as archives of past seawater chemistry (Erhardt et al. 2020).

5.3. Snapshots of seawater δ^7Li values from ancient shallow-water marine carbonate sediments

The δ^7Li value of ancient shallow-water marine carbonates depends on both the mineralogy of the primary precipitate as well as the diagenetic conditions associated with the transformation of the primary sediment to carbonate rock. The systematic covariation between δ^7Li values and other carbonate-bound geochemical proxies (e.g., $\delta^{44/40}$Ca, δ^{26}Mg, Sr/(Ca + Mg)) in bulk-rock samples permits a robust approach that can deconvolve the effects of mineralogy and early marine diagenesis and provide a snapshot of seawater chemistry (e.g., the δ^7Li value of ancient seawater).

When applied to bulk carbonate sediment δ^7Li values, the data from this paper fall into three categories. First, samples that have low $\delta^{44/40}$Ca values (<-1.2 ‰), elevated Sr content, and a range in δ^7Li values up to 12 ‰. These reflect aragonite-dominated sediment altered under sediment buffered conditions with respect to calcium. Second, samples with intermediate $\delta^{44/40}$Ca values (~-1‰), elevated Li/(Ca-Mg) and Mg/(Ca + Mg) ratios, and a range in δ^7Li values up to 6 ‰. This signature suggests primary sediment dominated by HMC and altered under relatively sediment-buffered conditions with respect to Ca. In both cases, the most elevated δ^7Li values may approach the δ^7Li value of seawater, though unless the full 12 ‰ (for primary aragonite) or 6 ‰ (for primary HMC) range in δ^7Li values is captured, estimates of past seawater δ^7Li values will have greater uncertainty. Third, samples characterized by elevated $\delta^{44/40}$Ca values (>-0.8 ‰), very low Sr/(Ca + Mg) ratios, and uniform δ^7Li values. Samples of this type may have had either aragonite- or HMC-dominated primary sediment that has been transformed to diagenetic calcite/dolomite under fluid-buffered conditions. In this case, the δ^7Li values likely directly record the δ^7Li value of seawater.

The δ^7Li value of seawater is best constrained when sample suites capture the full range of diagenetic conditions from

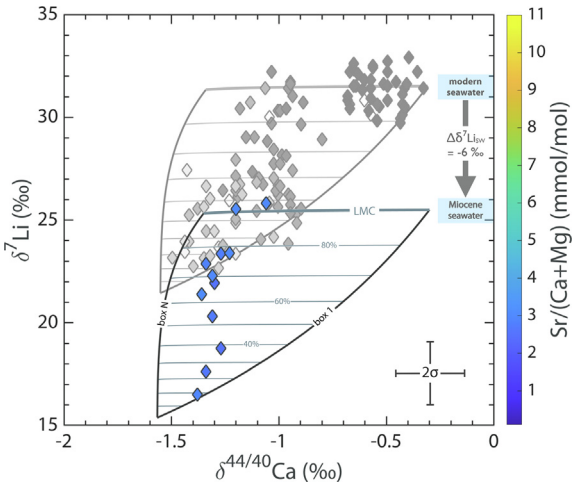

Fig. 8. Model results for neomorphism of Bahamian platform sediment (93 % aragonite, 7 % HMC) to LMC in the presence of Early Miocene (15–23 Ma) seawater, with measured core samples from the Early Miocene section of 1003, plotted as δ^7Li vs $\delta^{44/40}$Ca values. Samples are colored by measured Sr/(Ca + Mg) ratios. Also plotted in grey are model results for neomorphism of platform sediment (93 % aragonite, 7 % HMC) to LMC by modern seawater and measured data for all Bahamian late Miocene-to-Pleistocene core samples (darker grey represents lower Sr/(Ca + Mg) ratios. See Fig. 6).

sediment-buffered to fluid-buffered – i.e., span the full range of the model phase space (Fig. 4). In lithium isotope space, this will be a range of ~ 12 ‰ for primary sediment composed of predominantly aragonite (e.g., the Bahamas) and ~6 ‰ for primary sediment composed predominantly of HMC (e.g., site 1131). Calcium isotopes will have a range ~1.3 ‰ (−1.5 ‰ to −0.2 ‰) and ~ 0.8 ‰ (−1.0 ‰ to −0.2 ‰) for aragonite and HMC sediment, respectively. While the primary and diagenetic endmember isotopic compositions of the rock may vary with past secular changes to the isotopic composition of seawater, the range in isotopic composition between these endmembers will be independent of the isotopic composition of seawater.

Early Miocene (~16–23 Ma) samples from the deepest ~ 300 m of Site 1003 demonstrate how our approach can be applied to reconstruct the δ^7Li value of ancient seawater. Fig. 8 shows model results fit to data from this section, where the only model parameter adjusted from Pliocene-Pleistocene conditions is a lower δ^7Li value for seawater. Collectively, the low $\delta^{44/40}$Ca values (<-1.2 ‰), moderately elevated Sr content (~3300 mmol/mol), and δ^7Li values ranging over ~ 10 ‰ of these samples suggest a primary aragonite composition and diagenetic conversion to LMC under relatively sediment-buffered conditions. The results suggest a δ^7Li value for early Miocene seawater of ~ 26 ‰ (~6‰ lower than modern seawater composition), consistent with independent records in planktonic foraminifera (Hathorne and James, 2006; Misra and Froelich, 2012) and brachiopods (Washington et al., 2020).

However, where sample suites do not show a full range of diagenetic alteration (e.g., sediment-buffered to fluid-buffered), the best targets to reconstruct the δ^7Li of seawater are samples with the most elevated $\delta^{44/40}$Ca values, and in the case of dolomites, uniform and low δ^{26}Mg values. The massive dolomites from Unda, SS, and LBB provide an illustration of this approach. These dolomites exhibit only a small fluid-buffered diagenetic range, indicated by elevated $\delta^{44/40}$Ca values, low and uniform δ^{26}Mg values, low Sr/(Ca + Mg) ratios, and δ^7Li values that are indistinguishable from modern seawater. We caution, however, that our results do not suggest that marine dolomites will always directly recover seawater δ^7Li values. For example, Crockford et al., 2021 examined a Tonian section of predominantly dolostones that capture sediment

dolomitized under a continuum of diagenetic conditions from fluid- to sediment buffered, preserving a ~ 12 ‰ range in dolomite δ^7Li values. In this case, a Tonian seawater δ^7Li value was inferred from the most elevated δ^7Li value.

The approach of using systematic co-variation between sets of carbonate-bound geochemical proxies to reconstruct snapshots of seawater chemistry from ancient marine carbonate sediments has both advantages and disadvantages. The primary disadvantage of this approach is its limited temporal resolution; the approach necessarily integrates records of seawater chemistry over millions of years – the timescale of early marine diagenesis – and thus likely cannot be used to reconstruct changes in δ^7Li_{sw} on shorter timescales. This approach also offers several advantages. First, as demonstrated above, this method can be applied to samples altered under either sediment-buffered (e.g., Miocene samples from Site 1003) or fluid-buffered conditions (e.g., late Neogene dolomites from Unda, LBB, and SS) and does not necessarily require careful screening for well-preserved primary minerals, a screening that in many cases is not possible due to the small scales where diagenetic alteration has been observed (μm scale; e.g. Husson et al., 2020; Ingalls and Snell, 2021). As a result, this method can be applied widely in the geologic record and the accuracy of inferred seawater δ^7Li values can be checked by reconstructing snapshots from multiple geographically dispersed locations with sediment of similar age. Additionally, since the apparent isotopic fractionation factors for lithium into diagenetic carbonate minerals is close to $\alpha \approx 1.000$ for both LMC and dolomites, our approach of utilizing altered samples to infer seawater composition removes the need to assume specific isotopic fractionation factors or assess vital effects associated with the precipitation of biogenic primary metastable minerals. This is especially advantageous as both experimental and empirical studies of lithium isotope fractionation into primary carbonates (aragonite, HMC, LMC) show a range of over 28 ‰ (Dellinger et al., 2018; Day et al., 2021).

6. Conclusion

Using a large data set of Li isotope measurements in Neogene shallow-water carbonate sediments from platform to slope environments we have shown that stratigraphic variability in bulk carbonate δ^7Li values – comparable in magnitude to the rise in the δ^7Li value of seawater over the Cenozoic as recorded in foraminifera and brachiopods – is caused by variations in both mineralogy and style of diagenetic alteration (fluid-buffered vs sediment-buffered). In addition, we show that by pairing measurements of bulk sediment δ^7Li values with independent geochemical indicators of mineralogy and diagenesis – $\delta^{44/40}$Ca values, δ^{26}Mg values, and element ratios – we are able to deconvolve the geochemical signals associated with mineralogy and diagenesis to produce robust 'snapshots' of ancient seawater δ^7Li values. While this approach can be applied to ancient sediment of any primary carbonate mineralogy (aragonite, LMC, or HMC) that has experienced any range in extent (%) of recrystallization or style of diagenesis (sediment- vs fluid-buffered), samples characterized as having undergone early diagenetic alteration under fluid-buffered conditions (as indicated by elevated $\delta^{44/40}$Ca values, low Sr content, and uniform δ^7Li values) provide the best target for reconstructing the δ^7Li value of seawater from ancient shallow-water carbonate sediments.

Research Data

Source code for the diagenesis model associated with this article can be accessed at *github.com/johnjackmurphy/Diagenesis-Model*.

Data availability

The data is available as supplementary material and a link to the model code is provided in the manuscript.

Declaration of Competing Interest

The authors declare that they have no known competing financial interests or personal relationships that could have appeared to influence the work reported in this paper.

Acknowledgements

We sincerely thank the reviewers for their time and thoughtful comments, which have helped to improve this manuscript. We would also like to thank Dario Marconi and Emily Geyman for providing seawater samples. We are grateful to Elizabeth Lundstrom and Nick Slater for lab assistance. This work was supported by a grant from the Simons Foundation (SCOL 611878, ASCA). JAH acknowledges support from NSF grant no. 1654571. The Clino and Unda cores were collected under NSF Grant OCE8917295 to PKS and R.N. Ginsburg.

Appendix A. Supplementary material

Supplementary material to this article can be found online at https://doi.org/10.1016/j.gca.2022.09.019.

References

Ahm, A.S.C., Bjerrum, C.J., Blättler, C.L., Swart, P.K., Higgins, J.A., 2018. Quantifying early marine diagenesis in shallow-water carbonate sediments. Geochim. Cosmochim. Acta 236, 140–159.
Banner, J.L., 1995. Application of the trace element and isotope geochemistry of strontium to studies of carbonate diagenesis. Sedimentology 42, 805–824.
Bastian, L., Vigier, N., Reynaud, S., Kerros, M.E., Revel, M., Bayon, G., 2018. Lithium Isotope Composition of Marine Biogenic Carbonates and Related Reference Materials. Geostand. Geoanalytical Res. 42, 403–415.
Bathurst, R.G.C., 1966. Boring algae, micrite envelopes and lithification of molluscan biosparites. Geol. J. 5, 15–32.
Bathurst, R.G.C., 1971. Carbonate sediments and their diagenesis: Developments in sedimentology, vol. 12. Elsevier, Amsterdam.
Blättler, C.L., Higgins, J.A., 2014. Calcium isotopes in evaporites record variations in Phanerozoic seawater SO_4 and Ca. Geology 42, 711–714.
Blättler, C.L., Miller, N.R., Higgins, J.A., 2015. Mg and Ca isotope signatures of authigenic dolomite in siliceous deep-sea sediments. Earth Planet. Sci. Lett. 419, 32–42.
Bohlin, M.S., Misra, S., Lloyd, N., Elderfield, H., Bickle, M.J., 2018. High-precision determination of lithium and magnesium isotopes utilising single column separation and multi-collector inductively coupled plasma mass spectrometry. Rapid Commun. Mass Spectrom. 32, 93–104.
Chan, L.H., Leeman, W.P., Plank, T., 2006. Lithium isotopic composition of marine sediments. Geochemistry, Geophys. Geosystems 7.
Crockford, P.W., Kunzmann, M., Blättler, C.L., Kalderon-Asael, B., Murphy, J.G., Ahm, A.-S., Sharoni, S., Halverson, G.P., Planavsky, N.J., Halevy, I., Higgins, J.A., 2021. Reconstructing Neoproterozoic seawater chemistry from early diagenetic dolomite. Geology 49, 442–446.
Darrenougue, N., De Deckker, P., Eggins, S., Payri, C., 2014. Sea-surface temperature reconstruction from trace elements variations of tropical coralline red algae. Quat. Sci. Rev. 93, 34–46.
Dawans, J.M., Swart, P.K., 1988. Textural and geochemical alternations in Late Cenozoic Bahamian dolomites. Sedimentology 35, 385–403.
Day, C.C., Pogge von Strandmann, P.A.E., Mason, A.J., 2021. Lithium isotopes and partition coefficients in inorganic carbonates: Proxy calibration for weathering reconstruction. Geochim. Cosmochim. Acta 305, 243–262.
Dellinger, M., West, A.J., Paris, G., Adkins, J.F., Pogge von Strandmann, P.A.E., Ullmann, C.V., Eagle, R.A., Freitas, P., Bagard, M.L., Ries, J.B., Corsetti, F.A., Perez-Huerta, A., Kampf, A.R., 2018. The Li isotope composition of marine biogenic carbonates: Patterns and mechanisms. Geochim. Cosmochim. Acta 236, 315–335.
Dellinger, M., Hardisty, D.S., Planavsky, N.J., Gill, B.C., Kalderon-Asael, B., Asael, D., Croissant, T., Swart, P.K., West, A.J., 2020. The effects of diagenesis on lithium isotope ratios of shallow marine carbonates. Am. J. Sci. 320, 150–184.
Dixon, E.E.L., Vaughan, A., 1911. The carboniferous succession in Gower (Glamorganshire), with notes on its fauna & conditions of deposition. Q. J. Geol. Soc. London 67, 477–571.

Eberli, G.P., Ginsburg, R.N., 1987. Segmentation and coalescence of Cenozoic carbonate platforms, northwestern Great Bahama Bank. Geology 15, 75–79.
Eberli, G., Swart, P., Malone, M., 1996. Bahamas transect. JOIDES J. 22, 27–X3.
Eberli, G.P., Swart, P.K., Malone, M.J., 1997. Leg 166, Proceedings of the Ocean Drilling Program, Initial Reports. Ocean Drilling Program, College Station, TX.
Eberli, G.P., 2000. The record of Neogene sea-level changes in the prograding carbonates along the Bahamas Transect-Leg 166 synthesis. Proc. Ocean Drill. Progr. Sci. Results 166, 167–177.
Erhardt, A.M., Turchyn, A.V., Bradbury, H.J., Dickson, J.A.D., 2020. The calcium isotopic composition of carbonate hardground cements: A new record of changes in ocean chemistry? Chem. Geol. 540, 119490.
Fantle, M.S., Higgins, J., 2014. The effects of diagenesis and dolomitization on Ca and Mg isotopes in marine platform carbonates: Implications for the geochemical cycles of Ca and Mg. Geochim. Cosmochim. Acta 142, 458–481.
Fantle, M.S., Tipper, E.T., 2014. Calcium isotopes in the global biogeochemical Ca cycle: Implications for development of a Ca isotope proxy. Earth-Science Rev. 129, 148–177.
Fantle, M.S., Barnes, B.D., Lau, K.V., 2020. The Role of Diagenesis in Shaping the Geochemistry of the Marine Carbonate Record. Annu. Rev. Earth Planet. Sci. 48, 549–583.
Feary, D.A., Hine, A.C., Malone, M.J., 2000. Leg 182. Proceedings of the Ocean Drilling Program, Initial Reports. In: Proceedings of the Ocean Drilling Program, 182 Initial Reports, pp. 1–82.
Folk, R.L., 1965. Some Aspects of Recrystallization in Ancient Limestones. Dolomitization Limestone Diagenesis.
Füger, A., Konrad, F., Leis, A., Dietzel, M., Mavromatis, V., 2019. Effect of growth rate and pH on lithium incorporation in calcite. Geochim. Cosmochim. Acta 248, 14–24.
Gabitov, R.I., Schmitt, A.K., Rosner, M., McKeegan, K.D., Gaetani, G.A., Cohen, A.L., Watson, E.B., Harrison, T.M., 2011. In situ δ^7Li, Li/Ca, and Mg/Ca analyses of synthetic aragonites. Geochemistry, Geophys. Geosystems 12.
Geyman, E.C., Maloof, A.C., 2019. A diurnal carbon engine explains 13 C-enriched carbonates without increasing the global production of oxygen. Proc. Natl. Acad. Sci. 116, 24433–24439.
Ginsburg, R.N., 2001. The Bahamas Drilling Project: Background and Acquisition of cores and logs. In: Subsurface Geology of a Prograding Carbonate Platform Margin Great Bahama Bank, pp. 3–13.
Gothmann, A.M., Bender, M.L., Blättler, C.L., Swart, P.K., Giri, S.J., Adkins, J.F., Stolarski, J., Higgins, J.A., 2016. Calcium isotopes in scleractinian fossil corals since the Mesozoic: Implications for vital effects and biomineralization through time. Earth Planet. Sci. Lett. 444, 205–214.
Gussone, N., Böhm, F., Eisenhauer, A., Dietzel, M., Heuser, A., Teichert, B.M.A., Reitner, J., Wörheide, G., Dullo, W.C., 2005. Calcium isotope fractionation in calcite and aragonite. Geochim. Cosmochim. Acta 69, 4485–4494.
Hall, J.M., Chan, L.-H., 2004. Li/Ca in multiple species of benthic and planktonic foraminifera: thermocline, latitudinal, and glacial-interglacial variation. Geochim. Cosmochim. Acta 68, 529–545.
Hall, J.M., Chan, L.H., McDonough, W.F., Turekian, K.K., 2005. Determination of the lithium isotopic composition of planktic foraminifera and its application as a paleo-seawater proxy. Mar. Geol. 217, 255–265.
Hathorne, E.C., Felis, T., Suzuki, A., Kawahata, H., Cabioch, G., 2013. Lithium in the aragonite skeletons of massive Porites corals: A new tool to reconstruct tropical sea surface temperatures. Paleoceanography 28, 143–152.
Hathorne, E.C., James, R.H., 2006. Temporal record of lithium in seawater: A tracer for silicate weathering? *Earth Planet*. Sci. Lett. 246, 393–406.
Higgins, J.A., Blättler, C.L., Lundstrom, E.A., Akhtar, A.A., Bradbury, H., Murray, S.T., Swart, P.K., Holmden, C., Bialik, O., Crüger Ahm, A.-S., 2018. Mineralogy, early marine diagenesis, and the chemistry of shallow-water carbonate sediments. Geochim. Cosmochim. Acta 220, 512–534.
Husson, J.M., Higgins, J.A., Maloof, A.C., Schoene, B., 2015. Ca and Mg isotope constraints on the origin of Earth's deepest δ^{13}C excursion. Geochim. Cosmochim. Acta 160, 243–266.
Husson, J.M., Linzmeier, B.J., Kitajima, K., Ishida, A., Maloof, A.C., Schoene, B., Peters, S.E., Valley, J.W., 2020. Large isotopic variability at the micron-scale in 'Shuram' excursion carbonates from South Australia. Earth Planet. Sci. Lett. 538, 116211.
Ingalls, M., Snell, K.E., 2021. Tools for Comprehensive Assessment of Fluid-Mediated and Solid-State Alteration of Carbonates Used to Reconstruct Ancient Elevation and Environments. Front. Earth Sci. 9.
Jacobsen, S.B., Kaufman, A.J., 1999. The Sr, C and O isotopic evolution of Neoproterozoic seawater. Chem. Geol. 161, 37–57.
Kalderon-Asael, B., Katchinoff, J.A.R., Planavsky, N.J., Hood, A.V.S., Dellinger, M., Bellefroid, E.J., Jones, D.S., Hofmann, A., Ossa, F.O., Macdonald, F.A., Wang, C., Isson, T.T., Murphy, J.G., Higgins, J.A., West, A.J., Wallace, M.W., Asael, D., Pogge von Strandmann, P.A.E., 2021. A lithium-isotope perspective on the evolution of carbon and silicon cycles. Nature 595, 394–398.
Kenter, J.A.M., Ginsburg, R.N., Troelstra, S.R., 2001. Sea-level-driven sedimentation patterns on the slope and margin. In: Subsurface Geology of a Prograding Carbonate Platform Margin Great Bahama Bank Special Publications of SEPM, pp. 61–100.
Kievman, C.M., 1998. Match between late Pleistocene Great Bahama Bank and deep-sea oxygen isotope records of sea level. Geology 26, 635–638.
Kinsman, D.J.J., 1969. Interpretation of Sr+2 Concentrations in Carbonate Minerals and Rocks. SEPM J. Sediment. Res. 39, 486–508.
Lechler, M., Pogge von Strandmann, P.A.E., Jenkyns, H.C., Prosser, G., Parente, M., 2015. Lithium-isotope evidence for enhanced silicate weathering during OAE 1a (Early Aptian Selli event). Earth Planet. Sci. Lett. 432, 210–222.
Lin, J., Liu, Y., Hu, Z., Chen, W., Zhang, L., Chen, H., 2019. Accurate Measurement of Lithium Isotopes in Eleven Carbonate Reference Materials by MC-ICP-MS with Soft Extraction Mode and 10 12 Ω Resistor High-Gain Faraday Amplifiers. Geostand. Geoanalytical Res. 43, 277–289.
Lisiecki, L.E., Raymo, M.E., 2005. A Pliocene-Pleistocene stack of 57 globally distributed benthic δ 18O records. Paleoceanography 20, 1–17.
Lowenstam, H.A., 1961. Mineralogy, O^{18} /O^{16} Ratios, and Strontium and Magnesium Contents of Recent and Fossil Brachiopods and Their Bearing on the History of the Oceans. J. Geol. 69, 241–260.
Marconi, D., Weigand, M.A., Sigman, D.M., 2019. Nitrate isotopic gradients in the North Atlantic Ocean and the nitrogen isotopic composition of sinking organic matter. Deep Res. Part I Oceanogr. Res. Pap. 145, 109–124.
Marriott, C.S., Henderson, G.M., Belshaw, N.S., Tudhope, A.W., 2004a. Temperature dependence of δ7Li, δ44Ca and Li/Ca during growth of calcium carbonate. Earth Planet. Sci. Lett. 222, 615–624.
Marriott, C.S., Henderson, G.M., Crompton, R., Staubwasser, M., Shaw, S., 2004b. Effect of mineralogy, salinity, and temperature on Li/Ca and Li isotope composition of calcium carbonate. Chem. Geol. 212, 5–15.
McNeill, D.F., Ginsburg, R.N., Chang, S.B.R., Kirschvink, J.L., 1988. Magnetostratigraphic dating of shallow-water carbonates from San Salvador, Bahamas. Geology 16, 8–12.
McNeill, D.F., Eberli, G.P., Lidz, B.H., Swart, P.K., Kenter, J.A.M., 2001. Chronostratigraphy of a prograded carbonate platform margin: a record of dynamic slope sedimentation, western great Bahama bank. In: Subsurface Geology of a Prograding Carbonate Platform Margin Great Bahama Bank Special Publications of SEPM, pp. 101–134.
Melim, L.A., Swart, P.K., Maliva, R.G., 2001. Meteoric and marine-burial diagenesis in the subsurface of great Bahama bank. In: Subsurface Geology of a Prograding Carbonate Platform Margin Great Bahama Bank, pp. 137–161.
Melim, L.A., Swart, P.K., Eberli, G.P., 2004. Mixing-zone diagenesis in the subsurface of Florida and the Bahamas. J. Sediment. Res. 74, 904–913.
Mills, J.V., DePaolo, D.J., Lammers, L.N., 2021. The influence of Ca:CO_3 stoichiometry on Ca isotope fractionation: Implications for process-based models of calcite growth. Geochim. Cosmochim. Acta 298, 87–111.
Misra, S., Froelich, P.N., 2009. Measurement of lithium isotope ratios by quadrupole-ICP-MS: Application to seawater and natural carbonates. J. Anal. At. Spectrom. 24, 1524–1533.
Misra, S., Froelich, P.N., 2012. Lithium Isotope History of Cenozoic Seawater : Changes in Silicate Weathering and Reverse Weathering. Science 335, 818–823.
Morse, J.W., Mackenzie, F.T., 1990. Geochemistry of sedimentary carbonates. Elsevier.
Murray, S.T., Higgins, J.A., Holmden, C., Lu, C., Swart, P.K., 2021. Geochemical fingerprints of dolomitization in Bahamian carbonates: Evidence from sulphur, calcium, magnesium and clumped isotopes. Sedimentology 68, 1–29.
Murray, S.T., Swart, P.K., 2017. Evaluating formation fluid models and calibrations using clumped isotope paleothermometry on Bahamian dolomites. Geochim. Cosmochim. Acta 206, 73–93.
Odum, H.T., 1950. The Biogeochemistry of Strontium. Yale University, New Haven, Conn.
Penniston-Dorland, S., Liu, X.M., Rudnick, R.L., 2017. Lithium isotope geochemistry. Rev. Mineral Geochem. 82, 165–218.
Pogge Von Strandmann, P.A.E., Jenkyns, H.C., Woodfine, R.G., 2013. Lithium isotope evidence for enhanced weathering during Oceanic Anoxic Event 2. Nat. Geosci. 6, 668–672.
Pogge Von Strandmann, P.A.E., Desrochers, A., Murphy, M.J., Finlay, A.J., Selby, D., Lenton, T.M., 2017. Global climate stabilisation by chemical weathering during the Hirnantian glaciation. Geochemical Perspect. Lett. 3, 230–237.
Pogge von Strandmann, P.A.E., Schmidt, D.N., Planavsky, N.J., Wei, G., Todd, C.L., Baumann, K.H., 2019. Assessing bulk carbonates as archives for seawater Li isotope ratios. Chem. Geol. 530, 119338.
Pogge von Strandmann, P.A.E., Kasemann, S.A., Wimpenny, J.B., 2020. Lithium and Lithium Isotopes in Earth's Surface Cycles. Elements 16, 253–258.
Reijmer, J.J., Swart, P.K., Bauch, T., Otto, R., Reuning, L., Roth, S., Zechel, S., 2009. A re-evaluation of facies on Great Bahama Bank I: new facies maps of western Great Bahama Bank. Int. Assoc. Sedimentol. Spec. Publ 41, 29–46.
Roberts, J., Kaczmarek, K., Langer, G., Skinner, L.C., Bijma, J., Bradbury, H., Turchyn, A. V., Lamy, F., Misra, S., 2018. Lithium isotopic composition of benthic foraminifera: A new proxy for paleo-pH reconstruction. Geochim. Cosmochim. Acta 236, 336–350.
Rollion-Bard, C., Vigier, N., Meibom, A., Blamart, D., Reynaud, S., Rodolfo-Metalpa, R., Martin, S., Gattuso, J.P., 2009. Effect of environmental conditions and skeletal ultrastructure on the Li isotopic composition of scleractinian corals. Earth Planet. Sci. Lett. 286, 63–70.
Rosenthal, Y., Field, M.P., Sherrell, R.M., 1999. Precise Determination of Element/Calcium Ratios in Calcareous Samples Using Sector Field Inductively Coupled Plasma Mass Spectrometry. Anal. Chem. 71, 3248–3253.
Shields, G., Veizer, J., 2002. Precambrian marine carbonate isotope database: Version 1.1. Geochem. Geophys. Geosyst. 3, 1–12.
Sorby, H.C., 1879. The structure and origin of limestones. Nature 19, 424–425.
Sproson, A.D., Pogge von Strandmann, P.A.E., Selby, D., Jarochowska, E., Frýda, J., Hladil, J., Loydell, D.K., Slavík, L., Calner, M., Maier, G., Munnecke, A., Lenton, T. M., 2022. Osmium and lithium isotope evidence for weathering feedbacks linked to orbitally paced organic carbon burial and Silurian glaciations. Earth Planet. Sci. Lett. 577, 117260.

Supko, P.R., 1977. Subsurface dolomites, San Salvador, Bahamas. J. Sediment. Petrol. 47, 1063–1077.
Swart, P.K., 2008. Global synchronous changes in the carbon isotopic composition of carbonate sediments unrelated to changes in the global carbon cycle. Proc. Natl. Acad. Sci. 105, 13741–13745.
Swart, P.K., Ruiz, J., Holmes, C.W., 1987. Use of strontium isotopes to constrain the timing and mode of dolomitization of Upper Cenozoic sediments in a core from San Salvador, Bahamas. Geology 15, 262–265.
Swart, P.K., Elderfield, H., Beets, K., 2001. The $^{87}Sr/^{86}Sr$ Ratios of carbonates, phosphorites, and fluids collected during the Bahamas Drilling Project Cores Clino and Unda: implications for dating and diagenesis. Subsurf. Geol. a Prograding Carbonate Platf. Margin, Gt. Bahama Bank Results Bahamas Drill. Proj. 70, 175–186.
Swart, P.K., Melim, L.A., 2000. The Origin of Dolomites in Tertiary Sediments from the Margin of Great Bahama Bank. SEPM J. Sediment. Res. 70, 738–748.
Swart, P.K., Oehlert, A.M., 2018. Revised interpretations of stable C and O patterns in carbonate rocks resulting from meteoric diagenesis. Sediment. Geol. 364, 14–23.
Swart, P.K., Reijmer, J.J.G., Otto, R., 2009. A re-evaluation of facies on Great Bahama Bank II: variations in the $\delta^{13}C$, $\delta^{18}O$ and mineralogy of surface sediments. Perspect. Carbonate Geol.: Tribute Career Robert Nathan Ginsburg. 41, 47–59.
Taylor, H.L., Kell Duivestein, I.J., Farkaš, J., Dietzel, M., Dosseto, A., 2019. Lithium isotopes in dolostone as a palaeo-environmental proxy – An experimental approach. Clim. Past Discuss. 15, 635–646.
Tomascak, P.B., Magna, T., Dohmen, R., 2016. Advances in Lithium Isotope Geochemistry. Springer International Publishing.
Vahrenkamp, V.C., Swart, P.K., Ruiz, J., 1988. Constraints and interpretation of 87 Sr/86 Sr ratios in Cenozoic dolomites. Geophys. Res. Lett. 15, 385–388.
Vahrenkamp, V.C., Swart, P.K., Ruiz, J., 1991. Episodic dolomitization of late Cenozoic carbonates in the Bahamas: evidence from strontium isotopes. J. Sediment. Petrol. 61, 1002–1014.
Veizer, J., Ala, D., Azmy, K., Bruckschen, P., Buhl, D., Bruhn, F., Garden, G.A.F., Diener, A., Ebneth, S., Godderis, Y., Jasper, T., Korte, C., Pawellek, F., Podlaha, O.G., Strauss, H., 1999. $^{87}Sr/^{86}Sr$, $\delta^{13}C$ and $\delta^{18}O$ evolution of Phanerozoic seawater. Chem. Geol. 161, 59–88.
Vigier, N., Rollion-Bard, C., Levenson, Y., Erez, J., 2015. Lithium isotopes in foraminifera shells as a novel proxy for the ocean dissolved inorganic carbon (DIC). Comptes Rendus - Geosci. 347, 43–51.
Wang, C., Reinhard, C.T., Rybacki, K.S., Hardisty, D.S., Ossa, O.F., Wang, X., Hofmann, A., Asael, D., Robbins, L.J., Zhang, L., Planavsky, N.J., 2021. Chromium isotope systematics and the diagenesis of marine carbonates. Earth Planet. Sci. Lett. 562, 116824.
Washington, K.E., West, A.J., Kalderon-Asael, B., Katchinoff, J.A.R., Stevenson, E.I., Planavsky, N.J., 2020. Lithium isotope composition of modern and fossilized Cenozoic brachiopods. Geology 48, 1058–1061.
Zhang, S., Henehan, M.J., Hull, P.M., Reid, R.P., Hardisty, D.S., Hood, A.V.S., Planavsky, N.J., 2017. Investigating controls on boron isotope ratios in shallow marine carbonates. Earth Planet. Sci. Lett. 458, 380–393.